BOSHOFF, ADAM JACOBUS

THE GOLD ADSORPTION PROPERTIES OF SHALY MATERIAL FROM BEATRIX GOLD MINE

MSc **UP** **1994**

The gold adsorption properties of shaly material from Beatrix Gold Mine

by

Adam Jacobus Boshoff

Submitted in partial fulfilment of the requirements

for the degree of **Master of Science**

in the Faculty of Science

University of Pretoria

December 1994

ABSTRACT

Shaly material from Beatrix Gold Mine has been found to be capable of adsorbing gold from cyanide solutions. Black shale bands occur in the reef zone at Beatrix Mine, but because of the mode of occurrence of the shale bands selective mining cannot be practised and ore delivered to the plant is contaminated by shale. Petrographical investigations and gold adsorption experiments were undertaken on samples of these shales, in an attempt to quantify their gold adsorption properties.

Mineralogically the shales comprise muscovite, chlorite, pyrophyllite, and chloritoid which suggest that the shale is a low grade metamorphic rock. Two types of carbonaceous material are present in low concentrations and resemble kerogen. The one type can be described as filamentous and the other as roundish. Many workers gave convincing evidence that kerogen from Witwatersrand rocks are of biogenetic origin and that it resembles coal in many respects.

Gold adsorption tests were done at Gencor Process Research Laboratories and also at the University of Pretoria. The aim of these experiments was to find a correlation between the propensity of a shale to adsorb gold and other properties such as its mineralogy and carbon content.

Gold adsorption experiments have shown that over time there is a drop in pH of the gold cyanide solutions. This is caused by decomposition of the phyllosilicates in the strongly alkaline solutions. Analysis of these solutions showed that high amounts of *Si* and *Al* are present. No *Mg* and *Fe* were detected in the solutions which suggests that any dissolved *Mg* and *Fe* precipitate immediately on the surface of the solids so that gold could co-precipitate with colloidal $Mg(OH)_2$ and $Fe(OH)_3$. It was found that a tendency exists for high gold adsorption values to be preferentially related to high percentages of FeO (corrected for pyrite) + MgO + Al_2O_3 (corrected for muscovite) in the shales.

Rank measurements done on the carbonaceous particles in the shales showed that they fall in the anthracite range. To relate gold adsorption to the rank of carbonaceous material, gold adsorption tests were done on coal of varying rank. These tests showed that anthracite has the highest propensity to adsorb gold. This suggests that the carbonaceous particles would have similar gold adsorption properties as anthracite. The lack of an obvious correlation between the propensity of a shale to adsorb gold and its carbon content is probably due to the fact that not all the carbonaceous particles are liberated during milling so that they can be brought into contact with the gold cyanide solution.

It is therefore concluded that gold is mainly adsorbed onto the carbonaceous particles in the shale with possible minor loss of gold due to co-precipitation of gold with $Mg(OH)_2$ and $Fe(OH)_3$.

SAMEVATTING

Dit is bekend dat skalie van Beatrix-goudmyn die vermoë het om goud uit sianiedoplossings te adsorbeer. Swart skalie kom voor in die rifsone van Beatrix-myn, maar weens die dungelaagde aard daarvan kan selektiewe mynbou nie toegepas word nie. Erts wat die aanleg bereik, is dus met skalie gekontamineer. Petrografiese ondersoek van en goudadsorpsie-eksperimente op monsters van hierdie skalies is gedoen om hulle vermoë om goud te adsorbeer te probeer kwantifiseer.

Mineralogies bestaan die skalie o.a. uit muskoviet, chloriet, chloritoïed en piroffiliet, en hierdie mineraalversameling dui op 'n lae graad van metamorfose van die skalie. Twee tipes koolstofryke materiaal is in die skalies teenwoordig en albei kom ooreen met kerogeen. Die eerste kan beskryf word as veselagtig en die ander as ronderig. Getuienis van vroëere ondersoeke dui daarop dat die kerogeen in Witwatersrandgesteentes van biogenetiese oorsprong is en dat dit in baie opsigte met steenkool ooreenkom.

Goudadsorpsietoetse is deur die Gencor Proses Navorsingslaboratoriums en ook by die Universiteit van Pretoria gedoen. Die doel van hierdie eksperimente was om 'n korrelasie te vind tussen die vermoë van 'n skalie om goud te adsorbeer en ander eienskappe soos sy mineralogie en koolstofinhoud.

Tydens die goudadsorpsie-eksperimente was daar met verloop van tyd 'n daling in die pH van die goudsianiedoplossings. Dit is veroorsaak deur die ontbinding van die fillosilikate in die sterk alkaliese oplossings. Analise van dié oplossings het getoon dat hulle hoë konsentrasies van *Si* en *Al* bevat. Geen *Mg* en *Fe* is in die oplossings gevind nie wat daarop dui dat enige opgeloste *Mg* en *Fe* dadelik presipiteer op die oppervlak van die vaste stowwe, sodat goud moontlik saam neerslaan met kolloidale $Mg(OH)_2$ en $Fe(OH)_3$. Dit is gevind dat daar 'n neiging bestaan dat hoë goudadsorpsiewaardes verband hou met hoë persentasies FeO(gekorrigeer vir piriet) + MgO + Al_2O_3 (gekorrigeer vir muskoviet) in die skalie.

Rangbepalings op die koolstofryke deeltjies in die skalie dui daarop dat hulle in die antrasietgebied val. Om die goudadsorpsie te koppel aan die rang van die koolstofhoudende materiaal is goudadsorpsietoetse gedoen op steenkool van variërende rang. Dit is bevind dat antrasiet die hoogste vermoë tot goudadsorpsie het. Dit dui daarop dat die koolstofryke deeltjies 'n goudadsorpsievermoë soortgelyk aan antrasiet behoort te hê. Die gebrek aan 'n klaarblyklike korrelasie tussen die goudadsorpsievermoë van 'n skalie en sy koolstofinhoud kan moontlik toegeskryf word aan die feit dat al die koolstofryke deeltjies nie tydens maling vrygestel word nie en gevolglik nie in aanraking is met die goudsianiedoplossing nie.

Die gevolgtrekking word dus gemaak dat die goud hoofsaaklik op die koolstofryke deeltjies in die skalie geadsorbeer word, maar dat 'n ondergeskikte goudverlies kan voorkom weens die kopresipitasie van goud met $Mg(OH)_2$ en $Fe(OH)_3$.

CONTENTS

LIST OF FIGURES

LIST OF TABLES

1. INTRODUCTION

At most gold mines there is a loss of gold that starts underground during the physical extraction of the ore and continues to the chemical processes within the gold extraction plant. De Waal (1982) discussed the mineralogical and geological factors which have a deleterious influence on the recovery of gold during the metallurgical processing of the ore. One of these may be gold loss due to the presence of shale in the plant. Various workers such as Hausen and Buchnam (1984); Osseo-Assare, Afenya and Abotsi (1984), Abotsi and Osseo-Assare (1986,1987); Krendelev, Zhmodic and Mironov (1978); Enzweiler and Joekes (1990,1991); Logan (1986); Urban, Urban and Lloyd (1972) showed that shale can absorb gold from cyanide solutions, but not all material classified as shale absorbs gold and those that do, do so at different rates and to different gold loadings.

Kilian (1976; in Holtum, 1990) suggested that both adsorption and absorption took place during gold absorption testwork on shale form Leslie Gold Mine, and this has been confirmed during initial testwork on shale from Beatrix Gold Mine. Schaekers (1988; in Holtum, 1990) showed that washing of a gold loaded shale with a weak cyanide solution removed about 40% of the gold and that washing in a strong cyanide solution did not remove any more gold. Holtum (1990) suggests that the gold remaining on the shale after washing is very strongly adsorbed onto the carbon in the shale as desorption tests with activated carbon showed no desorption of the gold (Holtum and Penny, 1982; in Holtum 1990).

1.1 Purpose of investigation

Shale from the reef zone at Beatrix Gold Mine has been found to be capable of adsorbing gold from cyanide solutions, but because of the mode of occurrence of the black shale bands within the reef zone, selective mining cannot be practised and ore delivered to the plant is contaminated by shale. The aim of this investigation was to identify the phases in Beatrix shale which are responsible for gold adsorption and to quantify the effect of shale properties on potential gold loss during the leaching of gold ore by cyanide solutions.

Techniques which have been used to treat carbonaceous ores in which the carbon is suspected to adsorb gold include: (i) roasting or chemical oxidation to decompose carbonaceous materials; (ii) flotation to reject carbon; (iii) the use of kerosene or other reagents to passivate the adsorptive carbon compounds; (iv) carbon or resin in pulp; (v) flotation of a bulk concentrate which is treated by one of the above methods; and (vi) the use of chelating agents which have a stronger affinity for gold than the carbon in the ore (Guy, 1981). It was however beyond the scope of this study to investigate mechanisms that would inhibit or reduce the adsorption of gold from cyanide solutions by shale.

1.2 Locality of Beatrix Mine

Beatrix Gold Mine is located in the southern most portion of the Welkom goldfield in the Free State, about 30km south of Virginia (Fig. 1).

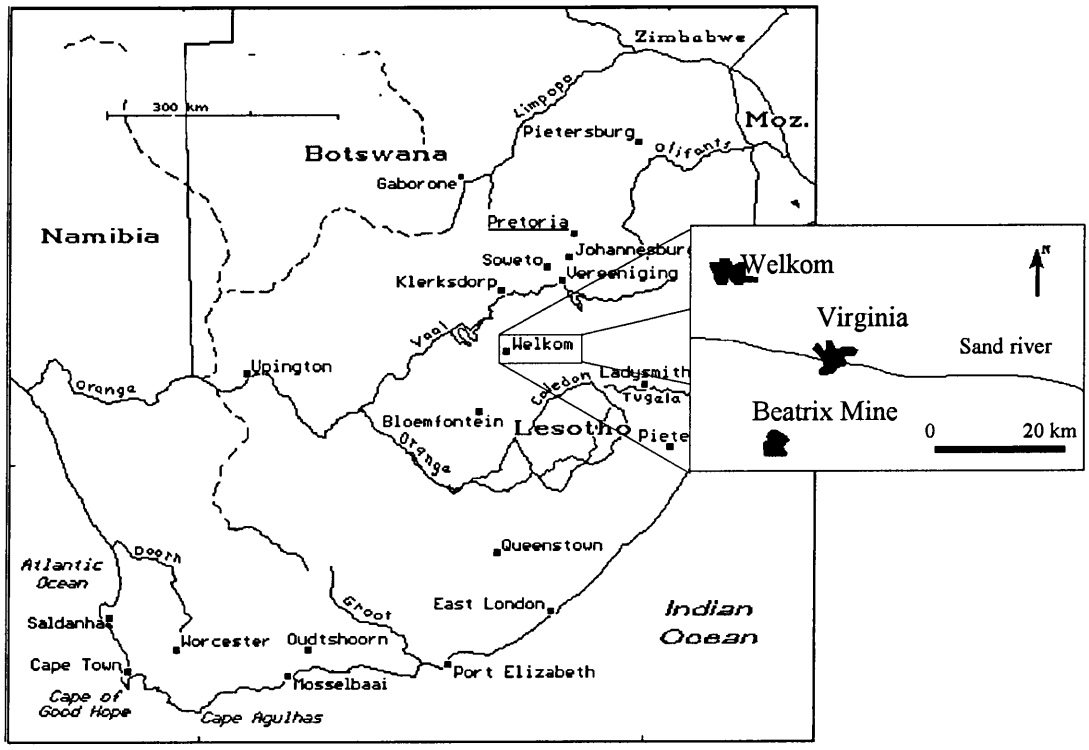

Figure 1 Locality of Beatrix Gold Mine

1.3 General geology

The 2800 to 2600Ma Witwatersrand Supergroup (SACS, 1980) lies unconformably on Archaean granites and schists and consists of a thick sequence of shales, quartzites and conglomerates with one intercalated lava flow (the Crown Formation). The sequence is divided into a lower, predominantly argillaceous unit, the West Rand Group, and an upper predominantly arenaceous unit, the Central Rand Group. The latter carries the auriferous reefs. Volcanic rocks of the Ventersdorp Supergroup and sedimentary rocks of the Karoo Supergroup overlie the Witwatersrand Supergroup in the study area. The units of the Central Rand Group exposed in the Beatrix Mine are the Aandenk and Eldorado Formations. The Aandenk Formation comprises mainly a sequence of quartzite whereas the Eldorado Formation comprises a sequence of black shale, quartzite and massive conglomerates.

The main gold reserves at Beatrix Mine are in the Beatrix Reef which lies at the base of the Eldorado Formation. At its shallowest, in the northern part of the lease area, the Beatrix Reef is about 860m deep and increases to about 1400m in the south. The dip of the reef varies between 0° and 5° and its thickness from as little as 1cm to a maximum of over 3m. It comprises a thin sequence of oligomictitic conglomerate and quartz arenite that grades upwards into black shale. Bands of black shale of varying thickness are also developed within the reef zone. Figure 2 shows a simplified geological column of the Witwatersrand Supergroup in the Welkom goldfield and Figure 3 a generalised profile of Beatrix Reef at Beatrix mine.

1.4 Previous work

Shaly material with the ability to adsorb gold from cyanide solutions has been found on a world-wide basis and consensus on the phases in shale which are

responsible for the adsorption of gold has not been reached yet. Hausen and Buchnam(1984) concluded that organic carbon in the ores from Carlin in Nevada, and not the mineral phases (illite, montmorillonite, kaolinite and pyrophyllite), was responsible for the adsorption of gold. Osseo-Assare *et al.* (1984) reviewed previous testwork done on carbonaceous ores and also concluded that carbonaceous material in these ores adsorbed gold from cyanide solutions.

Krendelev, Zhmodik and Mironov (1978) conducted adsorption tests on goethite(iron oxide) and various layer-silicate minerals, and concluded that the minerals fall in the following sequence of gold uptake per unit surface: vermiculite>illite>kaolinite>montmorillonite>goethite. Enzweiler and Joekes (1990, 1991) showed that colloidal iron oxides can adsorb gold from colloidal solutions. In South Africa, Logan (1986) concluded that carbonaceous matter in shale samples from Leslie Gold Mine was responsible for gold adsorption. Urban, Urban, and Lloyd (1972) used radioactive tracers and suggested that the minerals in shale, rather than the carbonaceous material, were responsible for the adsorption of gold.

Numerous tests on shales from Beatrix Gold Mine were done by workers at Gencor Process Research Laboratories. Schaekers(1988; in Holtum, 1990) showed that washing of a gold loaded shale with a weak or strong cyanide solution removed about 40% of the gold and to remove 80-90% the shale had to be refluxed with an acetone solution for 48 hours. Holtum (1990) therefore suggested that the gold remaining on the shale after initial washing was probably strongly adsorbed on carbonaceous material in the shale.

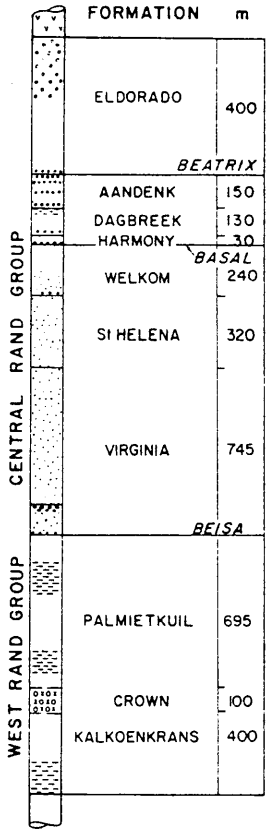

Figure 2. Simplified geological column of the Witwatersrand Supergroup in the Welkom goldfield. (Modified after Tweedie ,1986)

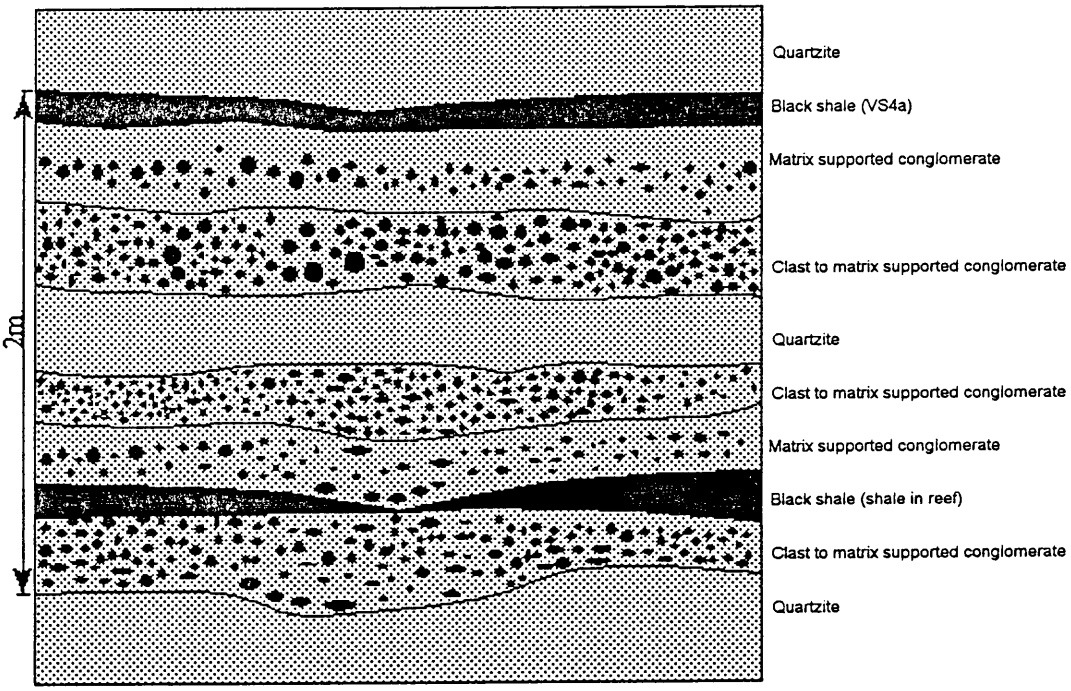

Figure 3. Generalised profile of Beatrix Reef at Beatrix Gold Mine

1.5 Methods of Investigation.

1.5.1 Sampling

In April 1993 eleven shale samples, designated *S1* to *S11*, from the reef zone at Beatrix Gold Mine were received. *S1* was not examined further as it was too small for any testwork. During a visit to Beatrix Mine in July 1993, a total of eight samples, designated *BX1* to *BX8*, were collected from the black shale bands within Beatrix Reef and also from the black shale band in the hangingwall. The sampling was done in such a way that localities close to basic dykes and sills and also some distance away from such intrusions were included. It is known that shale from Leslie Gold Mine also adsorb gold and a few samples of these shales were also collected (L1 - L4) to compare the gold adsorption properties of Leslie and Beatrix shales. All the samples were split into two subsamples, one for gold adsorption tests by Gencor Process Research Laboratories to assess its propensity to adsorb gold, and the other for investigation by the author at the University of Pretoria.

1.5.2 Gold adsorption experiments

Three types of experiments were done:

i) The shale samples were initially assessed by Gencor Process Research Laboratories using the standard Gencor procedure to quantify gold adsorption onto shale. This procedure involves exposing the shale to a stock solution of gold, containing about 8g Au/ton. After 24 hours of contact time the shale is assayed for gold after having been subjected to a rigorous standardised washing procedure (Gould ,1991).

ii) In analogy to work by Claassen (1991) on bacterial leaching of sulphide minerals, polished sections of shale on which carbonaceous particles had previously been circled by means of a diamond marker, were exposed to a 150g Au/ton cyanide solution for 48 hours that was constantly mixed by means of a magnetic stirrer. A Scanning Electron Microscope was then used to detect possible adsorbed gold on the particles. Before the SEM investigation the polished sections were washed with deionized water.

iii) Powdered shale (90%< 75μ) was added to gold cyanide solutions so that the solid:liquid ratio was 1:1 and stirred for 15, 30, 60 and 180 minutes respectively. The remaining solution and solids were then rapidly separated by means of a vacuum pump and a Buchner flask. The solids were subjected to a standardised washing procedure after which the gold concentrations of the washed solids were determined. The depleted cyanide- and washing solutions were also analysed for gold, iron, magnesium, silicon and aluminium by means of Atomic Absorption Spectrometry.

The latter experiment was also done on powdered coal samples of varying rank and on activated carbon to asses the effect of the rank of carbonaceous matter on gold adsorption.

1.5.3 Petrographic methods

A transmitted light microscope was used to determine the mineralogy of the shale samples on polished thin sections, polished with oil-based

diamond paste. By means of a counting grid the mineral proportions in the various samples were established. A representative portion of each sample was subjected to X-ray diffraction analysis to confirm the optical mineralogical determinations and to X-ray fluorescence spectroscopy to obtain the chemical compositions. Because of the very fine-grained nature of shale, an epinorm was also calculated to obtain a more consistent estimate of the mineral proportions.

To avoid oil contaminating the surface and inhibit gold adsorption during such experiments, polished sections of the specimens were prepared using water-based gamma-alumina polishing paste. The polished sections were examined under water immersion by using a reflected-light polarising microscope to locate, mark and examine carbonaceous material present in the samples. Reflectivity measurements (R_{max}) on the carbonaceous particles were done at the CSIR.

A microprobe was used to determine the composition of the various silicate minerals present in the shale. These data were then used to calculate the structural formulas of these minerals.

2. CHARACTERISTICS OF THE SHALE

2.1 Occurrence

The shaly material under investigation, are samples from black shale bands within and overlying the Beatrix Reef. The shale overlying the reef forms the hangingwall and is locally known as the *VS4a* shale (Fig.3). Table 1 gives the sample localities in relation to these bands of shale.

TABLE 1 Localities of various shale samples.

SAMPLE	LOCATION
S2	Shale in reef
S3	Shale in reef
S4	Shale in reef
S5	Shale in reef
S6	Shale in reef
S7	VS4a shale
S8	unknown
S9	unknown
S10	unknown
S11	unknown
BX1	Shale in reef
BX2	Shale in reef
BX3	Shale in reef
BX4	VS4a shale *
BX5	VS4a shale*
BX6	VS4a shale
BX7	Shale in reef
BX8	Shale in reef

*Shale close (about 20cm) to basic sill.

2.2 Macroscopical description

Both bands of shale can be described as laminated black carbonaceous shales (or slates) with the laminations varying between one and six millimetres. Close to basic dykes and sills the shale has been baked and displays slaty cleavage. Both shale bands have local variations in hardness and in places becomes very friable. The shaly material may also become very arenaceous so that it can then be described as a black siltstone.

Bands of rectorite are also developed in places. These bands of rectorite vary from a few centimetres to over 30cm in thickness and generally are lenticular in appearance. Rectorite is a swelling clay and this ability of the mineral to swell when wet and contract when dry complicates the underground operations at Beatrix Mine. The occurrence of the two shale bands is shown in Figures 4 and 5.

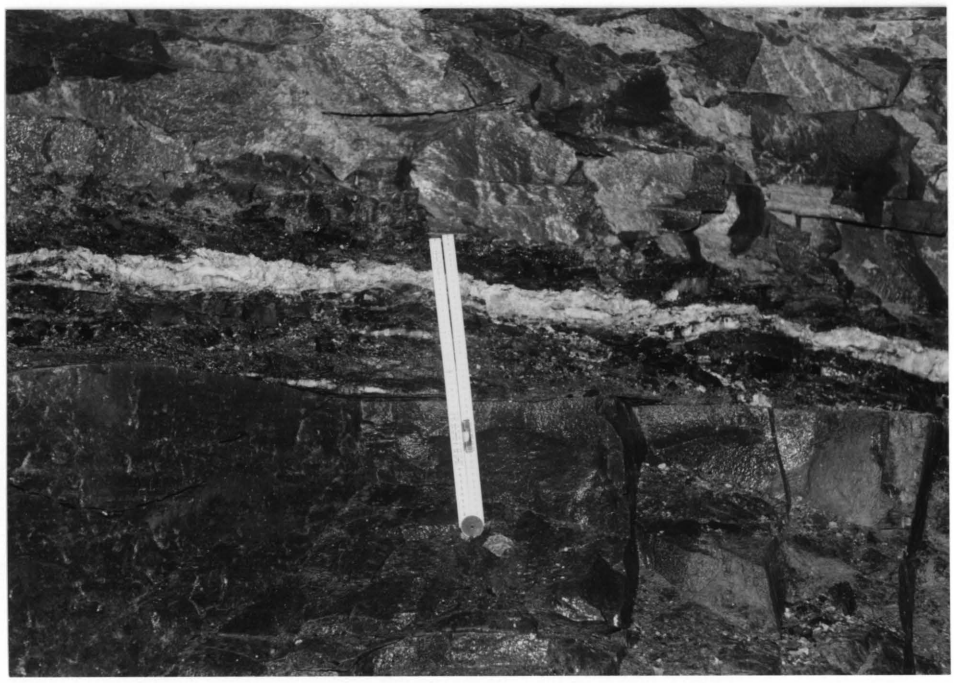

Figure 4. Black shale band within Beatrix Reef. The white band in the middle of the shale consists of rectorite.

Figure 5. VS4a shale in the hangingwall of Beatrix Reef. Note the quartz vein cutting through the shale at the top of the ruler.

2.3 Petrography

2.3.1 Introduction

The predominant silicate minerals identified in thin section are muscovite, chlorite, chloritoid and pyrophyllite that occur as small porphyroblasts indicating that the "shale" is a low grade metamorphic rock. The shales in contact with basic dykes and sills have been baked but displays no obvious change in mineralogy. A few detrital zircon crystals were also observed. The main oxide mineral is rutile whereas the main opaque minerals are pyrite and arsenopyrite. The matrix of the porphyroblasts is a clay sized mixture, probably of the minerals mentioned above, and in places thin bands of more arenaceous material can be seen in thin section (Fig. 6). Two types of carbonaceous material (or kerogen), containing varying amounts of uraninite, can be distinguished in polished sections. The one type can be described as filamentous (Fig. 11) and the other as roundish (Fig. 16).

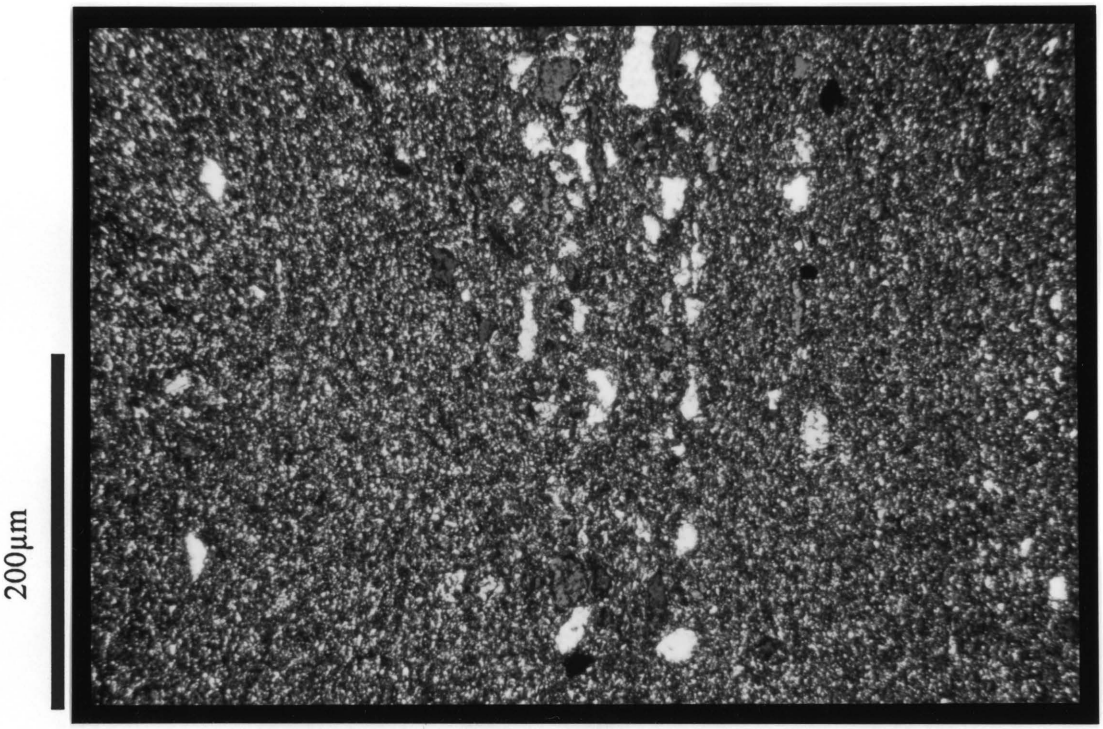

Figure 6. Typical appearance of Beatrix shale in thin section. Note the coarser bands of arenaceous material consisting of recrystallised quartz grains..

2.3.2 Silicate minerals

The muscovite that occurs as porphyroblasts is generally as disc shaped subrounded grains. They are commonly orientated parallel to the lamination (Fig. 7). Chlorite is almost exclusively intergrown with muscovite (Fig. 8) and sometimes replaces muscovite to a large extent. Chloritoid occurs as subidioblastic laths without preferred orientation and has grown across the laminated matrix (Fig 9). Pyrophyllite is commonly intergrown with quartz and to a lesser extent with muscovite, and under crossed nicols a colourful rim of pyrophyllite may be present around quartz grains (Fig. 10). Rectorite commonly appears as separate bands within the shale bands. Recrystallization textures are also prevalent causing the primarily rounded quartz grains to become sub-angular to angular in appearance.

Figure 7. Porphyroblasts of muscovite oriented parallel to the lamination. Lamination is NE-SW.

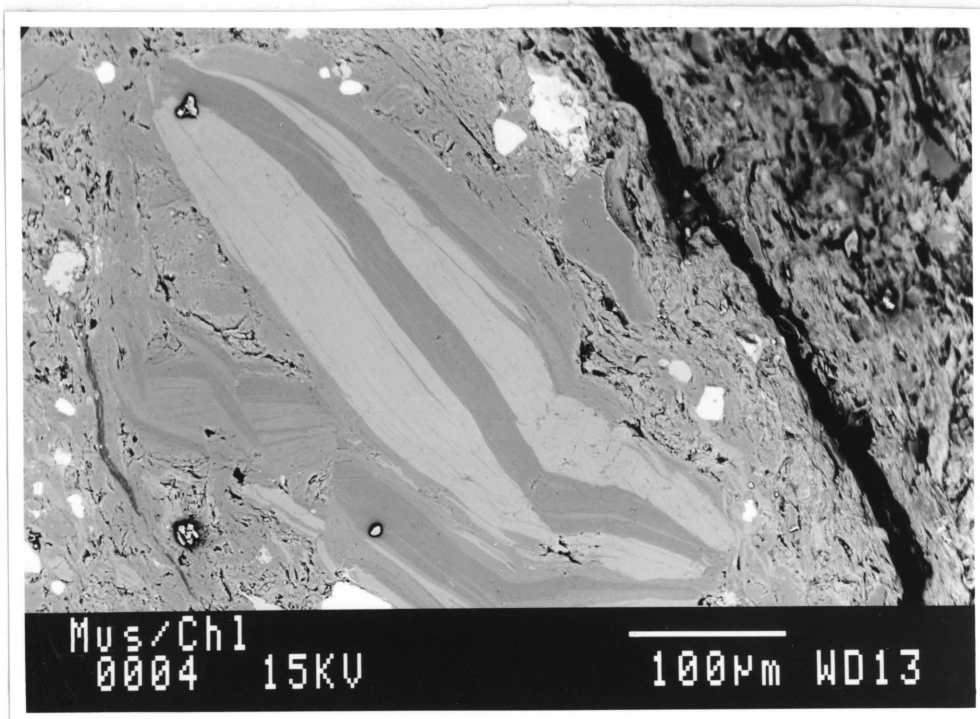

Figure 8. Backscatter electron-photomicrograph showing muscovite being replaced by chlorite. The darker area represents muscovite and the lighter area chlorite (higher average atomic number).

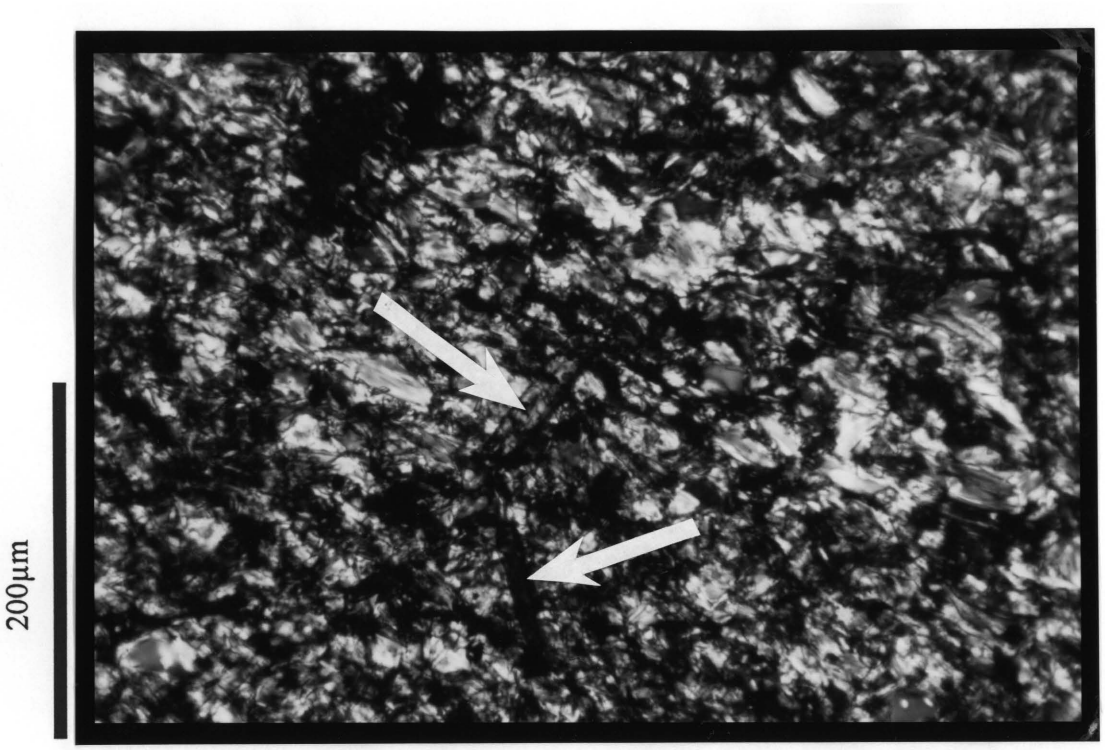

Figure 9. Chloritoid grains (arrows) which have overgrown the lamination.

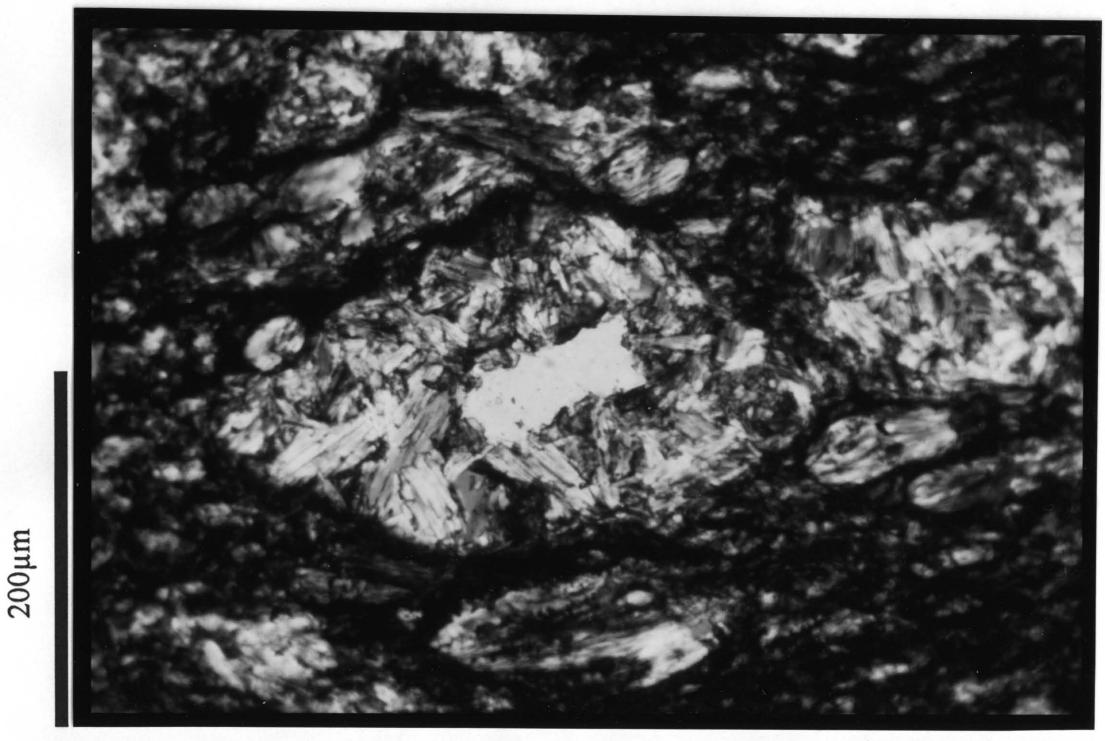

Figure 10. Colourful reaction rims of pyrophyllite around quartz grains

2.3.3 Carbonaceous material

The one type of carbonaceous material (kerogen) has a filamentous appearance while the other can be described as roundish. The kerogen is not dispersed homogeneously but appears to be concentrated along specific bedding planes. Logan (1986) reported that the carbonaceous material in shale from an East Rand gold mine was for the most part enclosed in chlorite. None of the carbonaceous particles observed in shale from Beatrix Mine was however found to be enclosed in a single mineral phase.

The carbonaceous particles exhibit a moderately strong reflection pleochroism and are weakly to moderately anisotropic under crossed nicols. Coalification haloes with a higher reflectivity and a stronger anisotropism than the rest of the material are present around small inclusions of uraninite. In this regard the carbonaceous particles closely resemble the kerogen of the Witwatersrand conglomerates.

The reflectivity (R_{max}) measured on different particles (with exception of the particles in shale close to basic sills) varies between 2.5% to 4.5% with an average of 3.8%. Even though specific care was taken to avoid zones close to coalification haloes, variations of up to one percent (R_{max}) were measured on single particles. A higher average value of 5.15% R_{max} was measured on carbonaceous particles in samples BX4 and BX5 as a result of the higher temperature close to a basic sill.

Filamentous carbonaceous particles

The short axes of these bodies vary between ca. 50µm and 300µm and their long axes between ca. 300µm and 1500µm. They are elongated and have a filamentous appearance (Fig. 11). The surface of one of these particles is shown in Figure 12. Finger-

like columns protruding from the side of one of these particles can be seen in Figure 13. Figure 14 shows the pitted and uneven structure of these particles. One of these pits is shown under high magnification in Figure 15. It shows an almost parallel arrangement of graphitoid laths in the carbonaceous particle.

Roundish carbonaceous particles

These bodies are more ore less round with jagged edges and have diameters of *ca.* 200µm to 500µm (Fig. 16 and 17). The roundish particles show many internal cavities (or pores) that vary in size from *ca.* 5µ to 80µ which may be filled by phases such as pyrite. Figure 18 shows the porous internal structure of a pore in a roundish carbonaceous particle. Small inclusions of uraninite surrounded by coalification haloes in a roundish particle are shown in Figure 19.

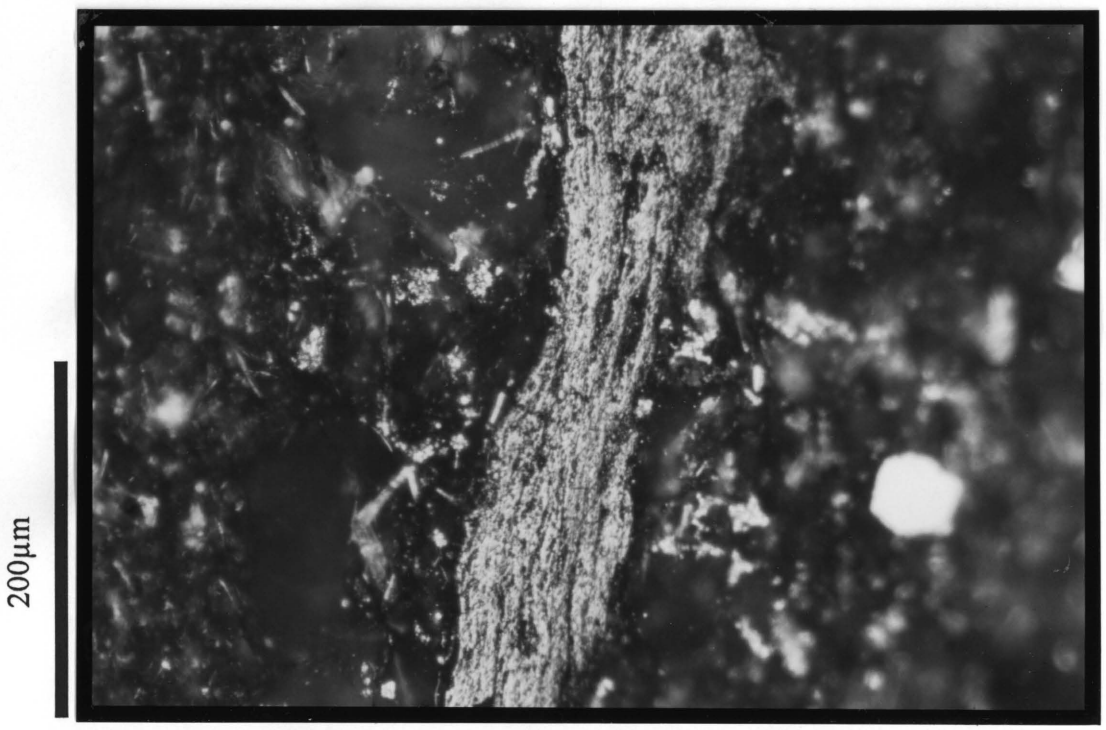

Figure 11. Filamentous carbonaceous particle.

Figure 12. The surface of a filamentous carbonaceous particle in which the filaments are clearly visible.

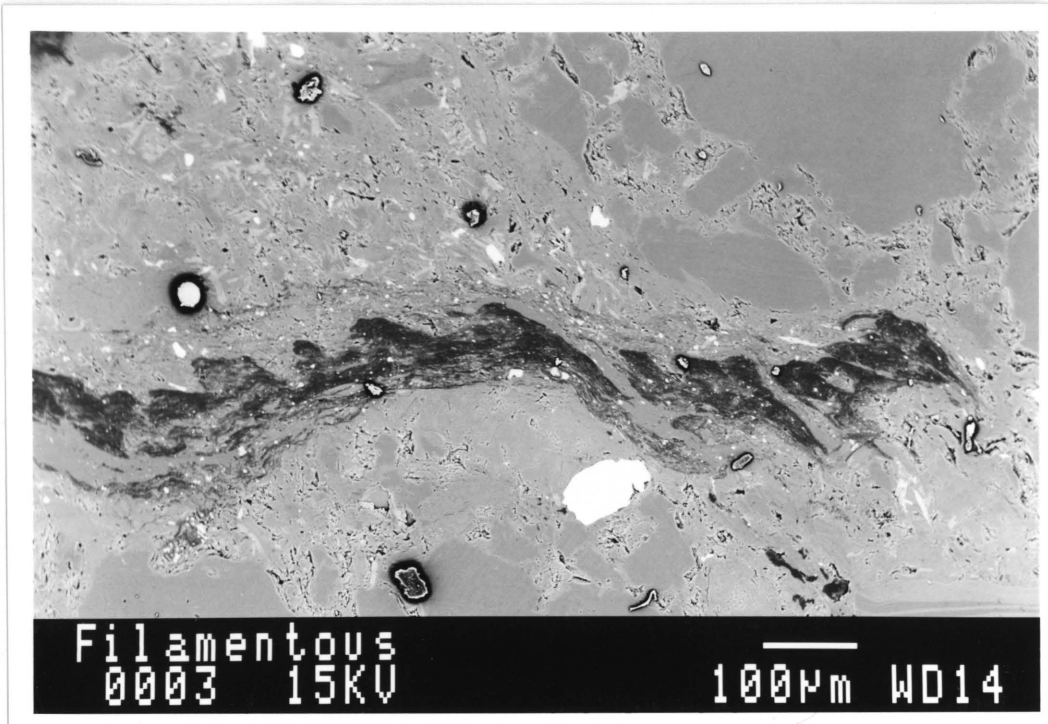

Figure 13. Backscatter electron -photomicrograph showing a filamentous carbonaceous particle (dark grey) with finger-like columns protruding from one side.

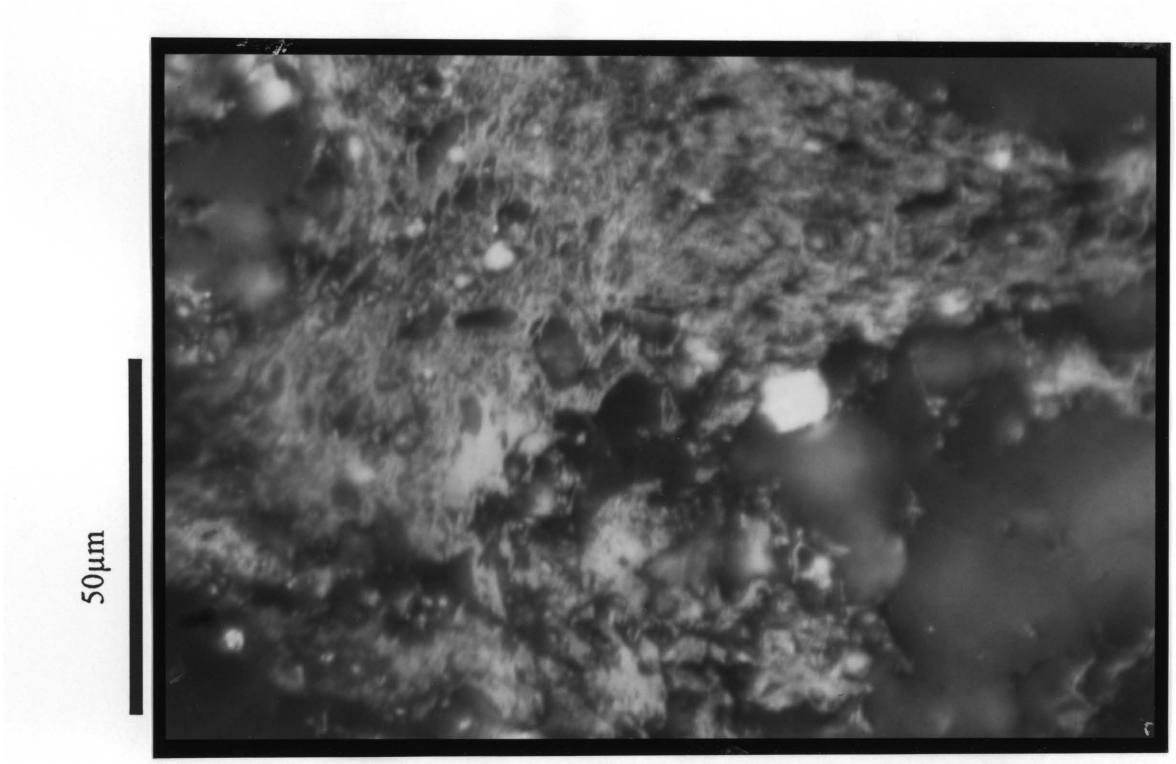

Figure 14. Pitted and uneven surface of a filamentous carbonaceous particle.

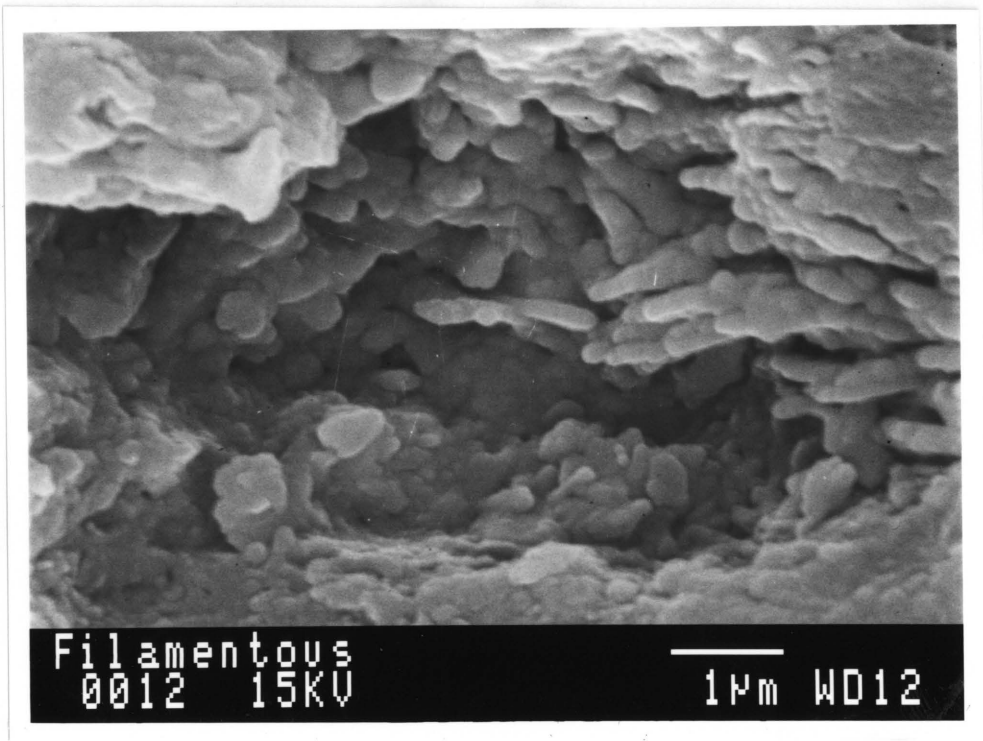

Figure 15. Electron-photomicrograph showing the internal structure of a pore in a filamentous carbonaceous particle. Note the quasi-parallel arrangement of "crystallites" of the carbonaceous material in the pore.

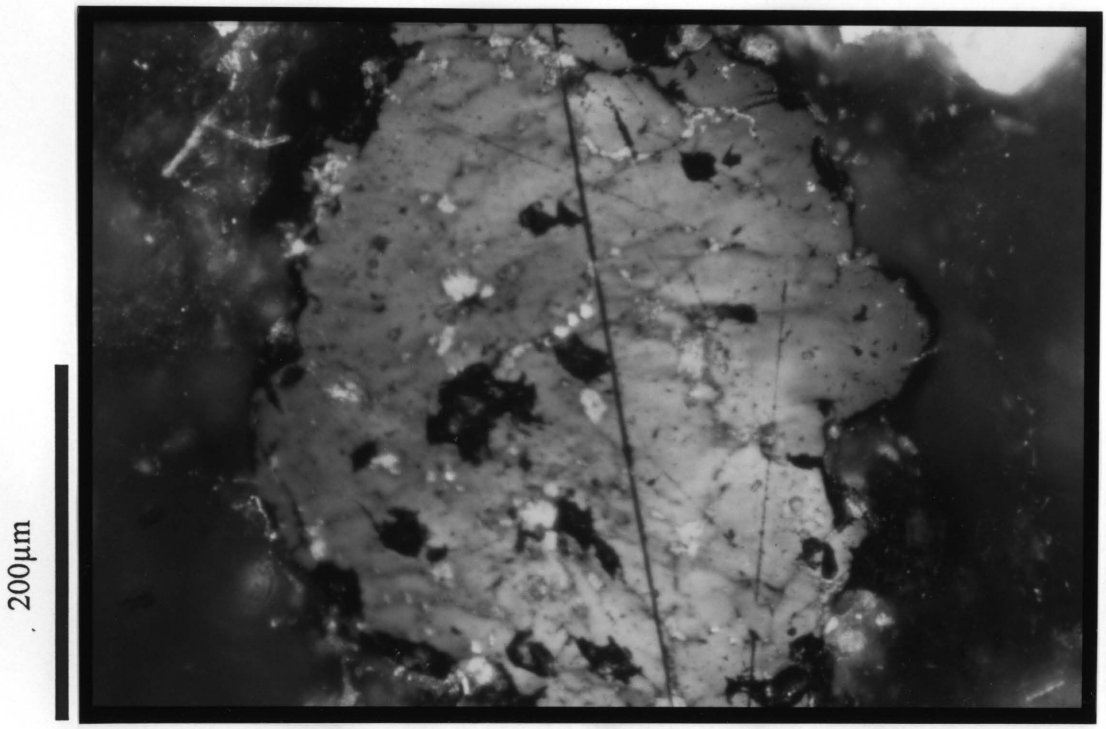

Figure 16. Roundish carbonaceous particle. Note the internal cavities (or pores) in the particle.

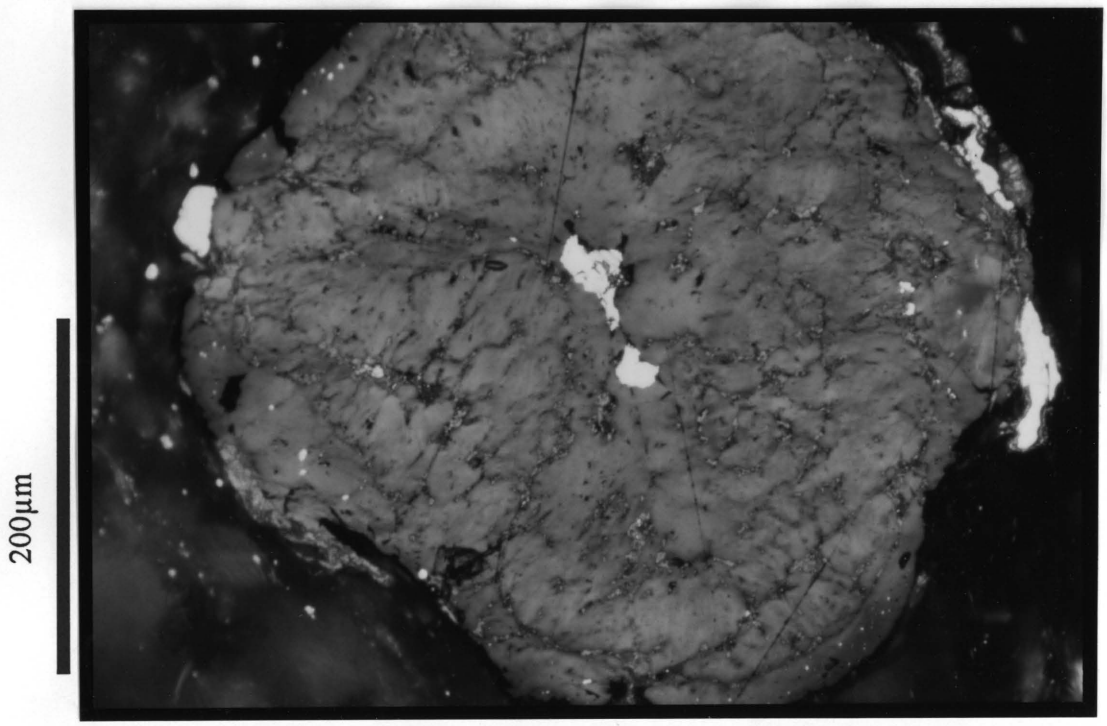

Figure 17. Roundish carbonaceous particle with more of the internal pores filled than the particle in Figure 16. The mineral filling the cavity in the centre of the particle is pyrite.

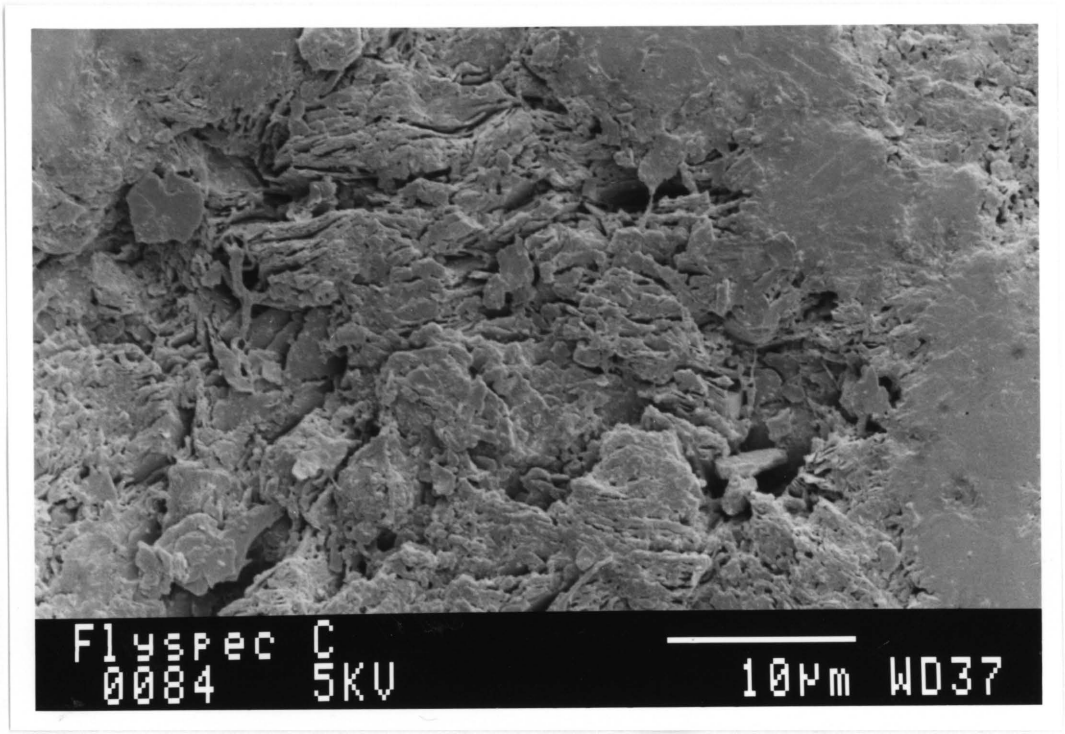

Figure 18. Electron-photomicrograph showing the internal structure of a pore in a roundish carbonaceous particle. Note the complex structure of the large pore due to irregularities of its surface caused by graphitoid crystallites.

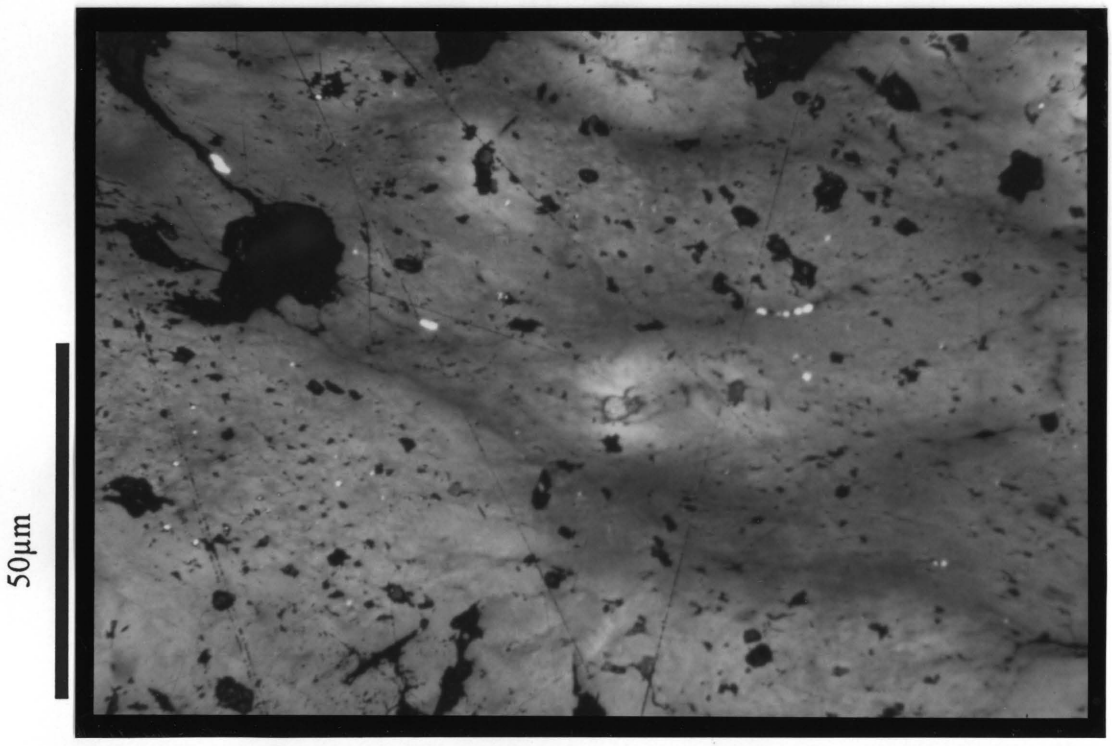

Figure 19. Coalification haloes (with a high reflectivity) around small inclusions of uraninite in a roundish carbonaceous particle.

2.4 Phase chemistry

The major silicate minerals (muscovite, chlorite, chloritoid, and pyrophillyte) were investigated with a microprobe to determine their compositions (Appendix 1) and structural formulas (Tables 2-5). The XRF analysis of sample BX1 (Appendix 2) was used to get an estimate of the composition of rectorite. Chemical analyses of Witwatersrand and other carbonaceous material from the literature were used to get an indication of the nature of the carbonaceous matter in Beatrix shale.

Muscovite

Muscovite is virtually the only *K*-bearing mineral in the shales. It may form at the lowest grades of metamorphism from the recrystallization of illite and clays (Guidotti, 1984). Since muscovite is fairly resistant to weathering it is possible that some of the grains in Beatrix shale may represent detrital particles. It has a high *K/Na*-ratio of 10.1 (Table 2) which indicates a low paragonite content. The respective values of the standard deviation show a fairly consistent composition for the muscovite in Beatrix shale. The ideal structural formula of muscovite can be written as:

$(K, Na, Ca)_2(Al,Mg,Fe,Cr,Ti)_4(SiAl)_8O_{20}(OH)_4$

Chlorite

The chlorite group of minerals derives its name from the green colour of most varieties. Chemically, the chlorites are hydrous silicates incorporating medium-sized octahedral cations, primarily *Mg*, *Al*, and *Fe*, but occasionally *Cr*, *Mn*, *Ni*, *V*, *Cu*, *Zn*, and *Li*. There is a continuous solid solution series between the Mg^{2+} and Fe^{2+} species. Most chlorites are trioctahedral and belong to the *Mg-Fe* series. The *Mg*-dominant species is named clinochlore with a structural formula of $(Mg_5Al)(Si_3Al)O_{10}(OH)_8$. The Fe^{2+}- dominant end member is chamosite with a structural formula $(Fe^{2+}{}_5Al)(Si_3Al)O_{10}(OH)_8$ (Bailey, 1988).

The average microprobe analysis of chlorite indicates that it is relatively *Al*-rich, and with a *Fe/Mg*-ratio of 1.37 (Table 3). However, the standard deviations for FeO and MgO indicate that there is probably variable mutual substitution of aluminium, iron and magnesium.

Chloritoid

Chloritoid is found most commonly in regionally metamorphosed rocks. The ideal composition of chloritoid is $FeO.Al_2O_3.SiO_2.H_2O$. The structure of chloritoid consists of two types of octahedral layers, one trioctahedral with the formula $[Fe_2^{2+} AlO_2(OH)_4]^-$ with *Mg* and *Mn* substitution for Fe^{2+} , and Fe^{3+} for *Al*; the other has a composition of $[Al_3O_8]^{-7}$ with three-fourths of the octahedral sites apparently filled only by *Al*. These layers are bound together by isolated $[SiO_4]$ tetrahedra whose basal planes are located over the empty octahedral sites in the $[Al_3O_8]^{-7}$ layer and whose apical oxygens are part of the trioctahedral layer. The two tetrahedral layers are related by centres of symmetry (Ribbe, 1982). The formula of chloritoid can therefore be written as:

$[(Fe^{2+}, Mg, Mn)_2 (Al, Fe^{3+})Al_3O_2[SiO_4]_2 [OH)_4]$

Chloritoid in Beatrix shale is *Fe*-rich with a *Fe/Mg*-ratio of 14 (Table 4). There is minor *Mn*, *Mg* and *Cr* substitution for Fe^{2+} and some *Al* substitution for Fe^{3+}. The low standard deviation values show that there is little variation in the composition of the chloritoid.

Pyrophyllite

Pyrophyllite is the dioctahedral form of the phyllosilicate group consisting of simple 2:1 layers. In the ideal case, no interlayer material exists in these structures because the 2:1 layers are electrostatically neutral. The primary forces holding the layers together are van der Waals bonds, which accounts for the soft nature of pyrophyllite. Pyrophyllite does not vary greatly in composition. On the basis of 22 positive charges per formula unit, a small but ubiquitous substitution of aluminium for silicon may occur. Octahedral sites are almost completely filled by more than 1.9 *Al* cations, supplemented by minor amounts of Fe^{2+}, Fe^{3+}, *Mg*,

and *Ti*. The general formula can be written as $Al_{2.0}(Si_{3.8}Al_{0.20})O_{9.8}(OH)_{2.2}$ (Evans and Guggenheim, 1988). Pyrophyllite is also the most aluminous rich phase in the shales and seems to be without any noteworthy cation substitution (Table 5).

Rectorite

Brown and Weir (1963; in Von Rahden *et al.* 1994) describe rectorite as a regularly interstratified mineral with equal proportions of mica-like and smectite-like interlayers where *Na, Ca, K,* and *Mg* can be present in both the mica-like and smectite interlayers. BX1 contains about 95% rectorite and according to the XRF analysis of this sample (Appendix 2) the interlayer cations are primarily *Na* and *Ca* with minor amounts of *K* and *Mg*.

Carbonaceous material (kerogen)

Because the grains of carbonaceous matter in Beatrix shale are very small and finely dispersed, it would be difficult to analyse it chemically. The analyses of carbonaceous matter from other Witwatersrand rocks (Hallbauer, 1986; Zumberge *et al.*, 1978) are therefore given in Tables 6-8. Hallbauer (1986) states that the *C/H* atomic ratios show a strong relationship between coal and the carbonaceous matter, and that the coal nature of the Witwatersrand carbonaceous matter is emphasized when average values of *C, O, H,* and *N* for kerogen are compared with average values for coal. This is also illustrated by Figure 20 in which the kerogen is seen to fall on the coalification line of macrinite. Zumberge *et al.*(1978) showed that the *C/H* -ratios for Vaal Reef kerogen falls into the petroleum asphaltene to low rank anthracite range.

Zumberge *et al.* (1978) did detailed investigations of the organic chemistry of kerogen from the Vaal Reef and the Carbon Leader Reef. They showed that the kerogen or carbonaceous matter is an insoluble random aromatic polymer which contains an unusually high amount of organic free radicals. After pyrolysis at 450°C , the components were identified by mass spectroscopy. Tables 7 and 8

450°C , the components were identified by mass spectroscopy. Tables 7 and 8 list the more important components *viz.* mainly alkyl-substituted aromatic compounds, low-molecular-weight aliphatic hydrocarbons, and minor amounts of aromatic sulphur compounds. Organic oxygen compounds, such as acetaldehyde, methanol, and acetone were found to be present in low concentrations. A large concentration of organic free radicals were shown to be present in Vaal Reef kerogen which probably originated from irradiation by radioactive uraninite within the carbonaceous material.

Abotsi and Osseo-Asare (1986) investigated carbonaceous matter in refractory carbonaceous gold ores from the Prestea Goldfied in Ghana. They attempted to extract humic acid by leaching the ore with a NaOH solution for 12 days. However, no quantitative extraction of a humic acid fraction was achieved. The hydrocarbons in the ground ore were extracted by leaching with benzene in a soxhlet extractor for 21 days. The extract was separated from the solvent by vacuum distillation. Infrared analysis of the hydrocarbon extract showed the predominance of CH_3, CH_2, CH and C=O groups, characteristic of long chain hydrocarbons and organic acids. To isolate the carbon fraction the ground ore was leached with hydrofluoric acid. After this leaching the remainder was also leached with H_2SO_4 to remove any AlF_3 formed. It was finally leached with HNO_3. They found that the organic matter consists primarily of hydrocarbon and carbon components.

They also investigated the surface chemistry of the carbonaceous ore and the carbon extract by means of electrophoretic mobility and gold uptake measurements and found that both the ore and carbon extract are negatively charged in the pH range 3 to 11, with the negative charge increasing with pH.

TABLE 2 Average electron-microprobe analysis and structural formula of muscovite

	Average	**Standard deviation**
SiO_2	49.20	4.38
CaO	0.30	0.28
Cr_2O_3	0.18	0.06
MgO	0.31	0.41
Al_2O_3	36.83	1.99
FeO	0.95	1.12
ZnO	0.01	0.01
Na_2O	0.59	0.36
MnO	0.00	0.00
K_2O	9.07	1.83
TiO_2	0.11	0.10
Total	97.55	
H_2O	2.45 (assumed)	

Number of cations on the basis of 24(O)

Si	6.43
Al	1.57
	8.00
K	1.51
Na	0.15
Ca	0.04
	1.70
Al	4.10
Mg	0.06
Fe	0.10
Cr	0.02
Ti	0.01
	4.29

Structural formula:

$(K_{1.51}Na_{0.15}Ca_{0.04})(Al_{4.10}Mg_{0.06}Fe_{0.10}Cr_{0.02}Ti_{0.01})(Si_{6.43}Al_{1.57})O_{20}(OH)_4$

TABLE 3 Average electron-microprobe analysis and structural formula of chlorite

	Average	**Standard deviation**
SiO_2	24.73	1.03
CaO	0.05	0.04
Cr_2O_3	0.21	0.04
MgO	10.85	2.38
Al_2O_3	28.91	1.26
FeO	27.02	2.07
ZnO	0.07	0.02
Na_2O	0.15	0.22
MnO	0.41	0.04
K_2O	0.40	0.28
TiO_2	0.03	0.02
Total	92.83	
H_2O	7.17 (assumed)	

Number of cations on the basis of 36(O)

Si	5.00
Al	3.00
	8.00
K	0.01
Al	3.88
Ca	0.01
Cr	0.03
Mg	3.26
Fe	4.56
Zn	0.02
Na	0.06
Mn	0.07
Ti	0.00
	11.90

Structural formula: $(Mg_{3.26}Fe_{4.56}Al_{3.88}Cr_{0.03}Zn_{0.02}Mn_{0.07})(Si_{5.00}Al_{3.00})O_{20}(OH)_{16}$

TABLE 4 Average electron-microprobe analysis and structural formula of chloritoid

	Average	**Standard deviation**
SiO_2	24.68	0.34
CaO	0.03	0.01
Cr_2O_3	0.29	0.03
MgO	0.93	0.56
Al_2O_3	41.50	0.51
FeO	24.32	0.02
ZnO	0.03	0.02
Na_2O	0.05	0.07
MnO	1.18	0.03
K_2O	0.01	0.01
TiO_2	0.02	0.01
Total	93.05	
H_2O	6.95 (assumed)	

Number of cations on the basis of 14(O)

Fe	1.68
Mg	0.12
Mn	0.08
	1.88
Al	4.04
Si	2.04

Structural formula: $(Fe^{2+}_{1.68}Mg_{0.12}Mn_{0.08})(Al_{1.04})(Al_3O_2)(Si_{1.02}O_4)_2(OH)_4$

TABLE 5 Average electron-microprobe analysis and structural formula of pyrophyllite

	Average	**Standard deviation**
SiO_2	67.57	0.73
CaO	0.08	0.02
Cr_2O_3	0.09	0.01
MgO	0.00	0.00
Al_2O_3	28.30	1.16
FeO	0.05	0.03
ZnO	0.03	0.03
Na_2O	0.05	0.12
MnO	0.01	0.02
K_2O	0.12	0.12
TiO_2	0.01	0.01
Total	96.32	
H_2O	3.69 (assumed)	

Number of cations on the basis of 12(O)

Si	4.00
K	0.01
Ca	0.01
Al	1.96
	1.98

Structural formula: $(Al_{1.96}K_{0.01}Ca_{0.01})Si_4O_{10}(OH)_2$

TABLE 6 Elemental composition of carbonaceous matter from Witwatersrand Rocks. (From Hallbauer, 1986)

Origin of Samples	Volatiles %	Moisture %	Ash %	Carbon %	Hydrogen %	Nitrogen %	Oxygen %	Sulphur %	Atomic Ratios		
									C/H	O/C	H/C
Carbon Leader, Blyvooruitzicht	9,3	1,5	50,2	40,81	1,71	0,14	4,09	1,55	1,99	0,08	0,50
Carbon Leader, Blyvooruitzicht	9,1	0,9	56,7	35,66	1,49	0,11	not detrm.	5,50*	1,99	—	0,50
Carbon Leader, Blyvooruitzicht (HF residue)	17,7	2,9	6,4	78,82	3,33	0,18	5,71	2,66	1,97	0,05	0,51
Carbon Leader, Western Deep Levels	not detrm.	1,3	11,5	78,96	4,01	0,08	2,70	1,45	1,64	0,03	0,61
Basal Reef, St Helena	10,5	1,0	53,8	38,63	1,69	0,08	not detrm.	9,61*	1,90	—	0,53
Vaal Reef, Vaal Reefs	10,1	0,8	32,0	59,95	2,53	0,09	2,27	2,36	1,97	0,03	0,51
Vaal Reef, Vaal Reefs	11,1	0,9	17,8	73,73	2,98	0,09	3,01	1,49	2,06	0,03	0,49

* Sulphur partly fixed to ash.

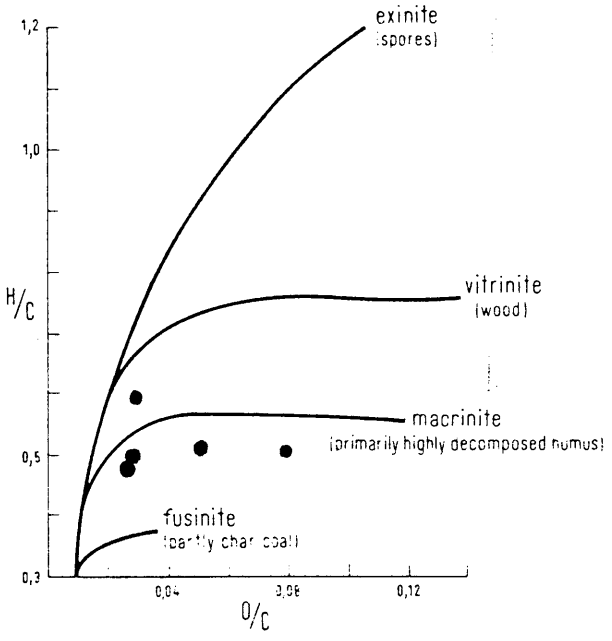

Figure 20. Plot of H/C : O/C atomic ratios(values from Hallbauer, 1986). Coalification tracks of the different macerals after van Krevelen (1961).

TABLE 7 Mass spectral identifications of major gas chromatic peaks (From Zumberge *et al.*, 1978)

Gass Cromatrographic Peak	Compound
1	toluene
2	2-methylthiophene
3	3-methylthiophene
4	ethylbenzene
5	*p*-xylene
6	*m*-xylene
7	*o*-xylene
8	*n*-propylbenzene
9	methylethylbenzene
10	methylethylbenzene
11	trimethylbenzene
12	methylstyrene
13	methylpropylbenzene
14	C_4-benzene
15	indene
16	methylindane
17	methylindane
18	methylindene
19	methylindene
20	naphthalene
21	benzothiophene
22	methyl-1,2-dihydronaphthalene
23	2-methylnaphthalene
24	1-methylnaphthalene
25	ethylnaphthalene
26	ethylnaphthalene
27	dimethylnaphthalene
28	dimethylnaphthalene
29	dimethylnaphthalene
30	dimethylnaphthalene
31	dimethylnaphthalene
32	propylnaphthalene
33	trimethylnaphthalene
34	trimethylnaphthalene

TABLE 8 Minor pyrolysis components identified by Gas Chromatography-Mass Spectrometry. (From Zumberge *et al.*,1978).

Aliphatic Hydrocarbons	Aromatic Hydrocarbons	Organic Sulphur Compounds
methylpropene	dimethylethylbenzenes	ethanethiol
pentene	C_5-alkylbenzenes	ethylthiophenes
methylpentane	C_6-alkylbenzenes	dimethylthiophene
methylcyclopentene	styrene	C_3-alkylthiophene
methylhexene	indane	C_4-alkylthiophene
C_7-alkane	C_2-alkylindanes	methylbenzothiophene
C_{10}-alkane	C_3-alkylindanes	C_2-alkylbenzothiophene
	C_4-alkylnaphthalenes	C_3-alkylbenzothiophene
	acenaphthene	dibensothiophene
		thiophenothiophene

2.5 Metamorphism

2.5.1 Introduction

Depending on the nature of weathering, shales consist of varying proportions of clay minerals (illite, montmorillonite, kaolinite), chlorite, detrital muscovite, occasionally some feldspar, and quartz which may be a major constituent. Calcite is often present, usually in minor amounts. Temperate weathering permits partial retention of the more mobile cations within the clay structure. Illite is formed in potassium-rich rocks whereas magnesium-rich rocks produce montmorillonite. Greater leaching of metal ions occur during tropical weathering which favours the formation of kaolinite. Extreme leaching removes even the silica, so that hydroxides of aluminium and iron are formed in stead of clay minerals.

Various changes of the clay minerals take place during diagenesis. This is in response to circulating fluids and slightly increased pressure. Irregular mixed-layer clay minerals such as montmorillonite are decomposed during advanced diagenesis and are therefore absent at the beginning of metamorphism. Quartz, chlorite , and illite are dominant and often are the only minerals in slates. This mineral assemblage is not diagnostic and may persist with increasing metamorphic grade, only the crystallinity of illite and kaolinite improves (Daira Duba and Williams-Jones, 1983).

The inclusion of organic matter in argillaceous rocks is largely controlled by the depositional environment. Where bottom conditions are oxidising, organic matter will be incorporated only where high rates of

sedimentation prevail. A greater retention of organic matter is achieved where conditions are reducing. These conditions probably prevailed during Witwatersrand times. Early diagenesis of organic matter is greatly influenced by the activity of bacteria which removes oxygen and nitrogen from proteins and carbohydrates and releases carbon dioxide, methane, and ammonia. The activity or presence of these organisms is not well understood for Witwatersrand times. If there is bacterial activity the residue would be rich in fatty acids and aminoacids and the further diagenesis involves the largely inorganic conversion of organic residues into hydrocarbons. Heating and burial cause distillation of the remaining hydrogen, leaving a progressively carbon rich residue.

2.5.2 Key metamorphic mineral phases

Pyrophyllite

Where *K*-feldspar and albite are absent in metapelites pyrophyllite may form as the typical metamorphic mineral at very low grade metamorphism (±325°C) (Winkler, 1976). Pyrophyllite may be formed by the reaction

$$\text{kaolinite} + \text{quartz} = \text{pyrophyllite} + \text{water}$$

Another possibility is the formation of pyrophyllite at the expense of muscovite through the ionic reaction

$$2\ \text{muscovite} + 6\ \text{quartz} + 2\ H^{+} = 3\ \text{pyrophyllite} + 2K^{+}$$

Evidence for the first reaction in Beatrix shale is the numerous reaction rims of pyrophyllite around quartz grains (Fig 10). Some muscovite flakes also showed reaction rims but evidence so far indicates that the second reaction is only of minor significance.

The first appearance of either andalusite or kyanite (depending on prevailing pressure) in quartz-bearing rocks requires that the upper stability of pyrophyllite has been reached or exceeded. The breakdown of pyrophyllite involves the following reaction:

pyrophyllite = andalusite/kyanite + quartz

Depending on pressure, the upper stability of pyrophyllite seems to be about 400-430° ± 15°C (Winkler, 1976). Since neither andalusite nor kyanite is present in the shales under investigation the upper stability boundary of pyrophyllite has not been reached. According to the formation of pyrophyllite a temperature constraint of between 300 to 400°C can be placed on the metamorphism of Beatrix shales.

Chloritoid

Under low grade metamorphic conditions chloritoid is formed in pelites which have a high *Fe/Mg* ratio, a relatively high *Al* content and simultaneously low contents of *K, Na,* and *Ca* (Winkler, 1976). The Beatrix shales seem to have a low content of the latter elements , are relatively aluminous and have an average *Fe/M*g ratio of 2.91 (standard deviation = 1.20) calculated from the geochemical data in Appendix 2. These shales therefore seem to have a suitable bulk composition for the formation of chloritoid. The following two reactions have been suggested

for the formation of chloritoid. The first one is probably responsible for the first appearance of chloritoid (Frey, 1972 in Winkler, 1976), whereas the second one may take place at slightly higher temperature:

pyrophyllite + iron-rich chlorite = chloritoid + quartz

hematite + iron-rich chlorite = chloritoid + magnetite + quartz

Rectorite

Von Rahden *et al.* (1994) recognised that the formation of rectorite always takes place in close proximity to quartz veins, faults or dykes. They suggest that the formation of rectorite did not depend on any thermal contribution from dykes, but that the faults, dykes and quartz veins provided channel-ways that acted as conduits along which hydrothermal fluids could move and infiltrate into existing argillaceous quartzite lenses and layers. Pre-existing phyllosilicates could then be altered to rectorite and Von Rahden *et al.* (1994) suggest that rectorite was formed at the expense of pre-existing pyrophyllite. According to Eberl and Howes (1977) the formation of rectorite takes place at temperatures of above 300°C.

2.5.3 Carbonaceous material

Organic material in sediments is very sensitive to a rise in temperature and pressure. It is more sensitive than silicate minerals, which explains the higher reflectivity of carbonaceous material close to basic intrusions without obvious mineralogical changes. Since the degree of coalification (rank) is an irreversible process, organic matter plays an important role in estimations of the degree of rock diagenesis and metamorphism.

The term coalification designates the development of organic matter from the peat stage through the stages of lignite, sub-bituminous coal, bituminous coal, anthracite and meta-anthracite to the stage of semi-graphite or graphitoid (Table 9). The degree of coalification is characterised by an increase in reflectance and carbon content as well as a decrease in volatile matter. Coalification therefore involves chemical and physical changes. The chemical changes are caused mainly by the increase in temperature and by the duration of heating whereas physical changes are caused mainly by lithostatic and/or tectonic pressure.

The most important chemical and structural changes in organic substances during coalification are illustrated diagrammatically in Figure 21. The hexagons in the uppermost row represent the aromatic rings and the lines are the aliphatic groups which, at higher rank stages, are gradually removed while the aromatic rings polymerize into larger clusters. Thus, coalification represents a rise of aromatization and of condensation. The second row of Figure 21 shows the increased orientation of the elementary molecular units parallel to the bedding plane.

Buseck and Huang Bo-Jun (1985) used high-resolution transmission electron microscopy to determine the structural changes that take place in non-crystalline organic matter in low-grade metamorphic rocks. They showed that in low grade metamorphic rocks, the carbonaceous units are relatively few in number, short in length and contorted. As metamorphic grade increases , the layers progressively increase in length and in number , the number of layers in the crystallite stack increases and the planarity of the layers increases.

TABLE 9 Coalification stages according to the German (DIN) and North American (ASTM) classification, as distinguished by different physical and chemical rank parameters. The last column shows the applicability of various rank parameters to the different coalification stages (From Stach et al., 1982).

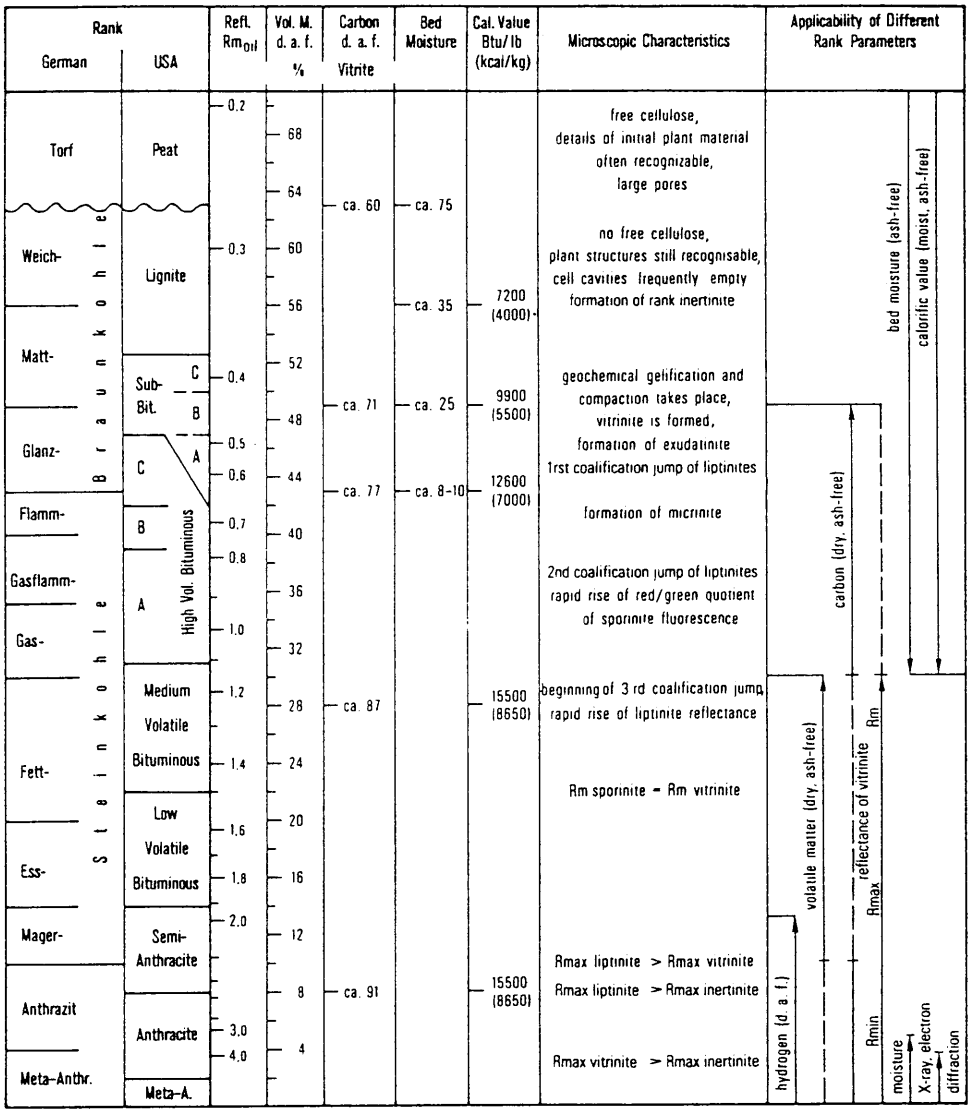

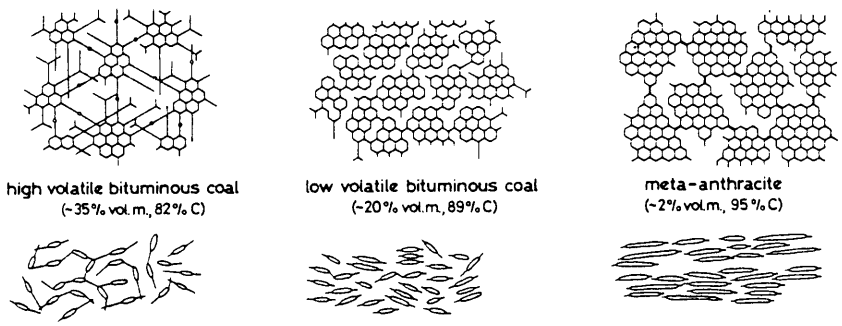

Figure 21 . Increase of aromatization and condensation, and ordering of the aromatic units parallel to the bedding plane during coalification of vitrinite (From Stach *et. al.* 1982)

There are many steps in the conversion of hydrocarbons into graphite. As polymerization proceeds to form larger, more complex carbon-rich units, hydrogen, nitrogen, and oxygen are lost. The ease of the pyrolytic conversion of organic compounds into graphite is a function of the structure and composition of the hydrocarbon precursors. If the structure is aliphatic (chain like structures) then they must first be aromatized (converted to ring like structures) before they can be polymerised into graphite-like molecules. A high initial content of aromatic compounds therefore greatly facilitates the formation of graphite-like molecules.

The chemical and physico-structural changes during coalification are not uniform but vary in the different rank stages. Different rank parameters are therefore used to determine the different rank stages. These rank parameters include chemical rank parameters and optical rank parameters to measure the chemical and physical changes associated with coalification. The most important chemical rank parameters include the carbon, oxygen, hydrogen, volatile matter and moisture content and the calorific value. The most important petrographic rank parameter is the optical reflectance which increases with rank. Figure 22 shows the relationship between vitrinite reflectance and different chemical rank parameters.

The correlation between temperature and coal rank is somewhat uncertain due to the lack of agreement as to the role of the duration of heating in coalification. Price (1983) suggested that age is not a controlling parameter of organic metamorphism and that a duration of heating of 1 Ma or more does not have a significant influence on maturation reactions

under conditions of burial metamorphism. For different sedimentary basins currently at or near maximum burial temperatures, with sediment burial times ranging from 2 to 240Ma, he showed that there is a strong correlation between reflectance and temperature (Figure 23), but no correlation between reflectance and burial (heating) times for any temperature interval.

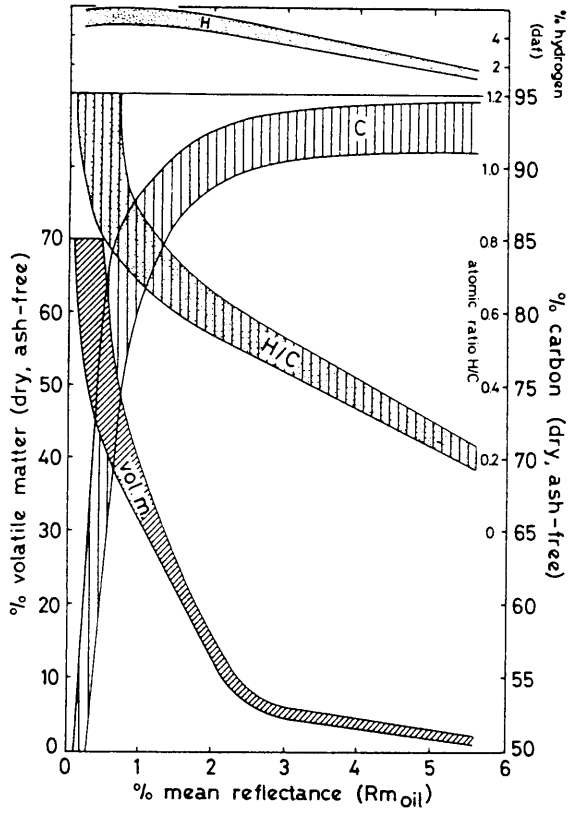

Figure 22. Relations between vitrinite reflectance and various chemical rank parameters (after Teicmhüller and Teichmüller, 1979)

R_{max} for the carbonaceous particles in Beatrix shale varies between 2.5% and 4.5% with an average of 3.8% which puts it in the semi-anthracite to anthracite range (Table 9). To plot these values in Figure 23, R_{max} must be converted to R_m. According to Ting (1978) the following relation exists in the case of high ranking coal:

R_{max} (maximum reflectance) = 1.066 x R_m (random reflectance)

R_m for the carbonaceous matter in Beatrix shale therefore varies between 2.35% and 4.22% with an average of 3.56%. According to Figure 23 the inferred temperature would be between 280 and 340°C with an average temperature of about 330°C.

The inferred temperature for the carbonaceous matter close to sills (R_m = 4.9%) is about 420°C. This suggests that the heating time of the basic intrusions was probably very short because they intruded at much higher temperatures. The carbonaceous material in the contact zone therefore did not have enough time to mature in accordance with the actual temperature. Further evidence for this relatively short period of heating is the absence of higher grade metamorphic minerals in these shales.

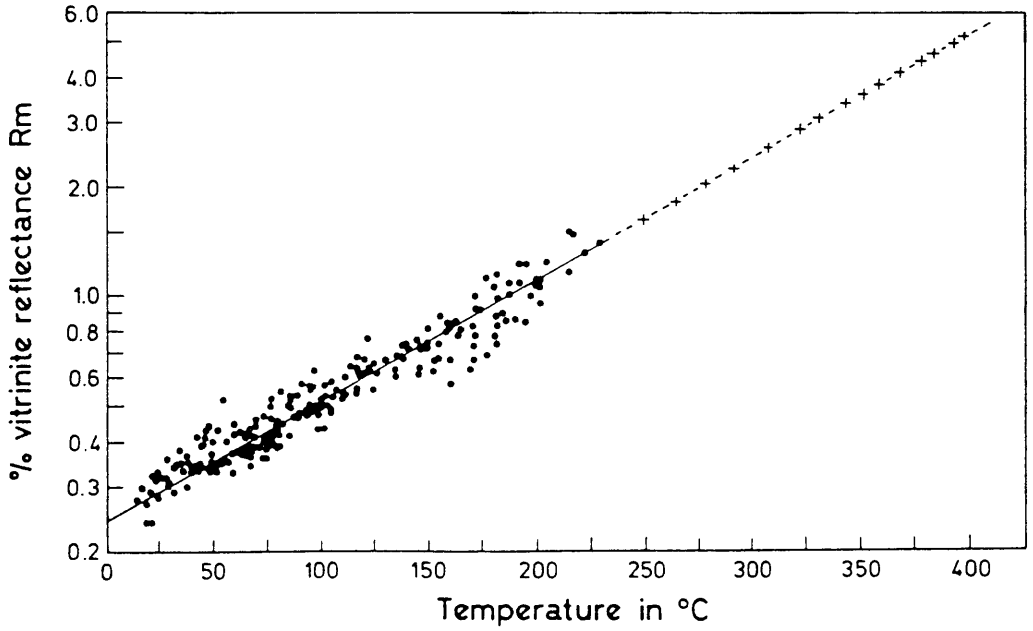

Figure 23. Plot of vitrinite reflectance *v.* burial temperature. Solid line is from a regression analysis of data from nine sedimentary basins in which the burial times range from 200 000 years to 240 million years. Dashed line is an extrapolation for five different basins. (Modified after Price, 1983, Figure 19).

2.5.4 Discussion of results

The metamorphic conditions deduced from the mineral assemblages and from the rank of carbonaceous material seem to be in agreement with each other, indicating metamorphic temperatures between 300 and 400°C for Beatrix shales. Phillips (1988) investigated shale samples from underground exposures from several Witwatersrand gold mines and concluded that the pelitic assemblages containing pyrophyllite, chloritoid and/or biotite suggest mid-greenshist facies with inferred metamorphic conditions of 350 ± 50°C and 1-2 kbar. Wallmach and Meyer (1990) constructed a petrogenetic grid for metamorphosed aluminous Witwatersrand shales that plot in the system Al_2O_3, SiO_2 and (Fe, Mg)O and suggest metamorphic conditions in the order of ±350°C and ±2.5kbar. According to Phillips (1988) more or less the same metamorphic conditions prevailed in all major Witwatersrand gold fields. The exceptions are outside the gold fields close to granite plutons where a higher metamorphic grade was achieved. Metamorphic conditions for the shale from Beatrix Mine seem to be in agreement with the inferred metamorphic conditions for other Witwatersrand shales in the goldfields.

2.6 Whole rock geochemistry

2.6.1 Inter- element variation

One of the most important objects of evaluating geochemical data is to ascertain the associations between the listed oxides and elements. This can be done by using the statistical technique of correlation. For this study the Spearman rank correlation coefficient was calculated for the major and trace elements in Appendix 2. The Spearman rank correlation coefficient is calculated as follows:

$$r_s = 1 - [\frac{6\sum D^2}{n(n^2 - 1)}]$$

where D is the difference in ranking between the *x*-values and *y*-values and n is the number of pairs. In this case the only assumptions are that *x* and *y* are continuous random variables, that they are at least ranked and are independent paired observations. If the rank orders are the same then D=0 and $r_s = +1.0$. If the rank orders are the reverse of each other then $r_s = -1.0$. The value of r_s therefore varies between -1.0 and +1.0.

Table 10 shows the correlation matrix for the major elements and Table 11 that for the trace elements. The correlation matrix for the trace elements versus major elements is shown in table 12.

TABLE 10 Spearman matrix of correlation for major elements.

	SiO_2	TiO_2	Al_2O_3	Fe_2O_3	MnO	MgO	CaO	Na_2O	K_2O	P_2O_5	Cr_2O_3	NiO
SiO_2	1.00											
TiO_2	-0.67	1.00										
Al_2O_3	-0.93	0.48	1.00									
Fe_2O_3	0.13	0.28	-0.48	1.00								
MnO	0.29	-0.08	-0.56	0.83	1.00							
MgO	0.11	0.01	-0.42	0.86	0.91	1.00						
CaO	0.04	-0.44	0.09	-0.40	-0.37	-0.29	1.00					
Na_2O	-0.19	-0.30	0.29	-0.43	-0.46	-0.32	0.94	1.00				
K_2O	-0.83	0.71	0.75	-0.10	-0.26	-0.17	-0.36	-0.09	1.00			
P_2O_5	-0.30	0.64	0.22	0.11	0.00	-0.12	-0.15	-0.17	0.41	1.00		
Cr_2O_3	0.11	0.51	-0.27	0.44	0.01	-0.02	-0.30	-0.32	0.02	0.28	1.00	
NiO	-0.13	0.47	-0.18	0.78	0.57	0.61	-0.28	-0.25	0.13	0.33	0.44	1.00

TABLE 11 Spearman matrix of correlation for trace elements.

	Zn	Cu	Ni	Ga	Mo	Nb	Zr	Y	Sr	Rb	U	Th	Pb	Co	Cr	V	Ba	Sc	S	As
Zn	1.00																			
Cu	0.42	1.00																		
Ni	0.76	0.74	1.00																	
Ga	-0.60	0.03	-0.22	1.00																
Mo	0.40	-0.08	0.26	-0.58	1.00															
Nb	0.31	0.34	0.58	0.19	0.48	1.00														
Zr	0.31	0.13	0.43	-0.17	0.82	0.81	1.00													
Y	0.39	0.53	0.55	0.10	0.11	0.56	0.37	1.00												
Sr	-0.49	-0.20	-0.40	0.46	-0.27	-0.19	-0.14	-0.07	1.00											
Rb	-0.27	0.09	0.17	0.63	-0.00	0.65	0.36	0.38	0.04	1.00										
U	0.58	0.18	0.25	-0.41	0.60	0.29	0.52	0.22	-0.24	-0.16	1.00									
Th	0.39	0.07	0.31	-0.17	0.74	0.68	0.88	0.39	-0.16	0.26	0.76	1.00								
Pb	0.51	0.08	0.27	-0.36	0.78	0.54	0.74	0.33	-0.16	-0.01	0.89	0.88	1.00							
Co	0.47	0.45	0.63	-0.12	0.59	0.70	0.82	0.49	-0.29	0.36	0.62	0.83	0.64	1.00						
Cr	0.68	0.26	0.44	-0.43	0.72	0.50	0.70	0.30	-0.35	-0.05	0.95	0.85	0.92	0.76	1.00					
V	0.06	-0.01	0.32	0.53	-0.05	0.68	0.34	0.47	-0.09	0.73	-0.17	0.29	0.01	0.33	0.00	1.00				
Ba	-0.30	-0.04	0.08	0.57	0.14	0.66	0.46	0.39	0.13	0.96	-0.12	0.36	0.11	0.36	-0.01	0.71	1.00			
Sc	0.05	-0.11	0.19	0.38	-0.31	0.23	-0.03	0.30	-0.10	0.48	-0.30	0.02	-0.26	0.10	-0.20	0.78	0.45	1.00		
S	0.29	0.05	0.15	-0.15	0.68	0.60	0.77	0.35	-0.06	0.20	0.81	0.92	0.92	0.69	0.83	0.13	0.32	-0.14	1.00	
As	-0.28	-0.06	0.02	0.35	0.31	0.39	0.60	0.13	0.13	0.50	0.16	0.56	0.23	0.62	0.24	0.37	0.55	0.21	0.40	1.00

TABLE 12 Spearman matrix of correlation of major *v.* trace elements.

	SiO_2	TiO_2	Al_2O_3	Fe_2O_3	MnO	MgO	CaO	Na_2O	K_2O	P_2O_5	Cr_2O_3	NiO
Zn	0.28	0.18	-0.59	0.93	0.73	0.74	-0.37	-0.43	-0.27	-0.05	0.61	0.67
Cu	-0.15	0.25	-0.05	0.56	0.38	0.38	-0.18	-0.12	0.10	0.17	0.22	0.74
Ni	-0.13	0.48	-0.21	0.90	0.66	0.73	-0.43	-0.37	0.17	0.25	0.38	0.89
Ga	-0.86	0.30	0.95	-0.48	-0.52	-0.37	0.23	0.42	0.60	0.06	-0.39	-0.22
Mo	0.27	0.43	-0.40	0.34	0.10	-0.01	-0.31	-0.37	0.06	0.54	0.76	0.30
Nb	-0.60	0.94	0.35	0.45	0.08	0.18	-0.42	-0.29	0.67	0.62	0.53	0.55
Zr	-0.21	0.80	0.04	0.33	-0.07	-0.02	-0.27	-0.23	0.40	0.68	0.73	0.49
Y	-0.42	0.52	0.18	0.47	0.35	0.41	-0.23	-0.14	0.38	0.29	0.30	0.75
Sr	-0.27	-0.21	0.37	-0.46	-0.47	-0.36	0.90	0.97	0.04	-0.01	-0.31	-0.27
Rb	-0.85	0.70	0.77	-0.10	-0.24	-0.14	-0.35	-0.08	1.00	0.37	-0.02	0.12
U	0.23	0.27	-0.34	0.34	-0.04	-0.06	-0.20	-0.21	-0.13	0.05	0.94	0.31
Th	-0.17	0.72	0.02	0.28	-0.19	-0.12	-0.27	-0.22	0.30	0.41	0.88	0.39
Pb	0.09	0.48	-0.24	0.36	-0.05	-0.05	-0.21	-0.22	0.04	0.29	0.94	0.33
Co	-0.24	0.74	0.03	0.45	0.03	0.10	-0.38	-0.30	0.39	0.45	0.75	0.67
Cr	0.14	0.47	-0.32	0.50	0.08	0.07	-0.33	-0.34	-0.02	0.24	0.99	0.47
V	-0.83	0.74	0.66	0.18	0.06	0.25	-0.33	-0.18	0.71	0.29	0.00	0.27
Ba	-0.81	0.71	0.74	-0.15	-0.30	-0.22	-0.28	-0.03	0.97	0.47	0.04	0.09
Sc	-0.56	0.33	0.45	0.12	0.16	0.30	-0.26	-0.16	0.44	0.05	-0.23	0.10
S	-0.12	0.58	0.02	0.16	-0.28	-0.25	-0.17	-0.12	0.25	0.33	0.88	0.28
As	-0.44	0.61	0.48	-0.29	-0.51	-0.46	-0.02	0.07	0.51	0.51	0.28	0.10

Major elements

The correlation between the major elements is largely dependent on the mineralogy of the shales. SiO_2 shows a strong negative correlation with Al_2O_3 and K_2O because a higher proportion of the aluminous minerals (pyrophyllite and muscovite) will result in a lower proportion of free SiO_2. There is a positive correlation between Al_2O_3 and K_2O because they are both incorporated in muscovite. The strong correlation between Fe_2O_3, MgO, MnO and NiO is caused by their incorporation in chlorite and chloritoid. CaO and Na_2O show a strong correlation because of their incorporation in muscovite and rectorite.

Trace elements

The correlation between the trace elements is determined by their mobility during weathering , diagenesis and metamorphism as well as their incorporation in the main minerals (Phillips ,1988). *Rb* and *Ba* have a good positive correlation because cations with large ionic radii, such as *Rb*, and *Ba* are often fixed in weathering profiles by preferential exchange and adsorption on clays. Smaller cations such as *Sr* are selectively leached from weathering profiles. There is for example a strong correlation between *Th* and *Zr* because of their incorporation in zircon and between *Rb* and K_2O because of the replacement of *K* by *Rb* in muscovite. The correlation between *U* and *Pb* suggests that the *P*b is of radiogenic origin.

2.6.2 Mineral proportions

Because the shales are very fine-grained it was not possible to determine the mineral proportions accurately by using a counting grid (11x11 points). Instead the chemical compositions (Appendix 2) of the shales were used to calculate an epinorm which should give mineral proportions consistent with the whole rock chemistry. In the calculation sodium and potassium are used to calculate the paragonite and muscovite contents respectively. The sulphur content was used with the appropriate amount of iron to form pyrite. The remaining iron was then

used to form iron chlorite. Magnesium was used in the formation of magnesium chlorite. As aluminium was used in the formation of all the above silicate minerals the remainder was allocated to pyrophyllite. The remaining silica represents quartz. Table 13 shows the normative mineral proportions of the various shale samples. For the sake of simplicity and because it seems to make out a small percentage of the minerals, chloritoid was not calculated and the Fe-chlorite should be considered to include chloritoid.

TABLE 13 Normative mineral percentages calculated from whole-rock chemistry (Appendix 2)

	Pyrite	Paragonite	Muscovite	Fe-Chlorite	Mg-Chlorite	Pyrophyllite	Quartz	Rutile	Total
L1	0.07	5.20	24.50	13.30	5.60	19.00	31.20	0.55	99.42
L2	0.98	7.20	25.60	1.29	1.80	56.60	1.79	0.95	96.21
L3	1.60	4.50	48.60	0.00	0.50	30.20	13.90	0.30	99.60
L4	0.10	5.42	31.50	8.20	6.84	9.94	36.10	0.80	98.90
S2	2.70	7.76	55.16	0.00	0.55	33.30	0.65	0.98	101.10
S3	0.98	6.16	26.53	1.29	1.71	58.92	1.79	0.95	98.33
S4	1.03	4.93	50.79	6.60	3.75	5.58	24.48	1.46	98.62
S5	1.86	5.55	57.38	6.29	3.12	4.70	17.53	1.89	98.32
S6	1.44	5.18	45.55	7.31	4.60	8.00	24.58	1.24	97.90
S7	0.20	3.70	38.95	8.97	4.41	23.55	17.22	1.16	98.16
S8	0.61	4.68	39.12	13.42	6.92	10.25	22.40	1.12	98.52
S9	0.10	5.42	32.53	7.60	6.84	9.94	35.96	0.67	99.06
S10	0.12	1.85	12.93	3.51	1.98	1.08	77.94	0.25	99.66
S11	0.19	3.20	20.45	5.97	3.61	5.66	59.19	0.54	98.81
BX1	0.22	21.69	6.25	0.00	1.16	32.40	32.39	0.20	94.31
BX2	0.36	6.16	41.49	0.00	0.50	48.61	0.20	1.00	98.32
BX3	0.16	5.42	24.34	0.00	0.33	65.19	1.47	1.00	97.91
BX4	0.13	2.96	11.91	10.31	10.01	10.20	53.94	0.76	100.22
BX5	0.07	4.81	23.49	12.30	4.63	18.51	30.32	0.55	94.68
BX6	0.17	7.03	32.70	8.30	0.41	17.93	29.23	0.84	96.61
BX7	0.06	8.14	63.88	0.49	4.60	25.53	0.10	0.76	103.56
BX8	1.01	7.77	55.18	0.00	0.55	32.30	0.81	0.96	98.58

Pyrite is present in low concentrations. It has the highest concentration in S2 and S5. All the sodium was used to calculate paragonite but if one takes into account that the average *K/Na*-ratio for muscovite in these shales is 10.01 then not all the sodium would be concentrated in paragonite. Some of the "paragonite" might therefore actually be rectorite because sodium can be present in the mica-like

interlayer and in the smectite-interlayer of rectorite. XRD analysis has shown that BX1 contains a high amount of rectorite which explains its high "paragonite" content.

Muscovite makes out the largest proportion of the phyllosilicates in most of the samples. The low muscovite content in BX1 is explained by its high rectorite content. The high pyrophyllite content of S3, BX2 and, BX3 imply a low alkali content in these samples.

Iron-rich chlorite (and chloritoid) is more abundant than magnesian chlorite (chloritoid) in most samples. In S3 and BX4 the amount of iron- and magnesium chlorite is about the same. In BX1, BX2, BX3 and, BX8 iron chlorite (chloritoid) seems to be absent which can be explained by the low iron content of these samples (Appendix I). Pyrophyllite in the shales generally tend to vary with alumina content and seems to reflect the high alumina and low alkali content of the samples.

The shales from Leslie Mine (L1 - L4) have compositions similar to those from Beatrix Mine.

3. GOLD ADSORPTION EXPERIMENTS

3.1 Introduction

One part of each sample was initially analysed at Gencor Process Research (GPR) laboratories to assess the propensity of the shales to adsorb gold. The other was subjected to gold adsorption experiments at the University of Pretoria. The aim of these tests was to quantify the ability of each shale to adsorb gold from cyanide solutions and to correlate this ability with other properties of the shales such as mineralogy and carbon content. Experiments by means of which mass balances could be calculated were also done at the University of Pretoria to determine if any gold is lost by possible precipitation on the glass ware used in the experiments.

3.2 Initial tests (Gencor)

The samples were milled to 80% < 75μ after which they were submersed in a 8g Au/ton gold cyanide solution for 24 hours. After a standardised washing procedure they were analysed for adsorbed gold. The organic carbon content of the shales was also determined by GPR. Some of the shales had an initial gold content of more than 0.5 g/ton and were leached with cyanide solution, containing suspended activated carbon prior to the adsorption tests. However, not all the gold could be removed and this made it difficult to interpret the results of these gold adsorption tests, because the gold loaded onto the shale can be confused with the residual gold not dissolved by the cyanide present in the solution during testing. Tables 14 and 15 show the gold adsorption results obtained from testwork at GPR.

With the exception of L4 all the samples show a propensity to adsorb gold. The gold adsorption displays a large variation, with S7 and BX6 having the highest values for Beatrix shales and L1 for Leslie shales. BX6, S8, S9, BX2, BX3, and BX8 all have values higher than 1g Au/ton.

TABLE 14 Results of gold adsorption tests on Beatrix shales.

Sample	Adsorption (g Au/ton)	Organic carbon (%)
S2	0.5	0.7
S3	0.1	0.2
S4	0.6	0.2
S5	0.2	0.2
S6	0.7	0.3
S7	6.8	0.5
S8	1.3	nd.
S9	1.5	nd.
S10	0.1	nd.
S11	0.5	nd.
BX1	0.1	0.2
BX2	1.8	0.5
BX3	1.0	0.3
BX4	0.7	0.7
BX5	0.2	0.4
BX6	3.3	0.3
BX7	0.5	0.4
BX8	1.4	0.7

nd. = not determined

TABLE 15 Results of gold adsorption tests on Leslie shales

Sample	Adsorption (Au g/ton)	Organic carbon (%)
L1	1.8	0.17
L2	0.2	0.04
L3	0.6	0.14
L4	0.0	0.05

It is evident from Figure 24 that there is no obvious correlation between carbon content and gold adsorption. However, in some cases such as S3, BX1, L2 and, L4 a low amount of gold adsorption is accompanied by a low carbon content.

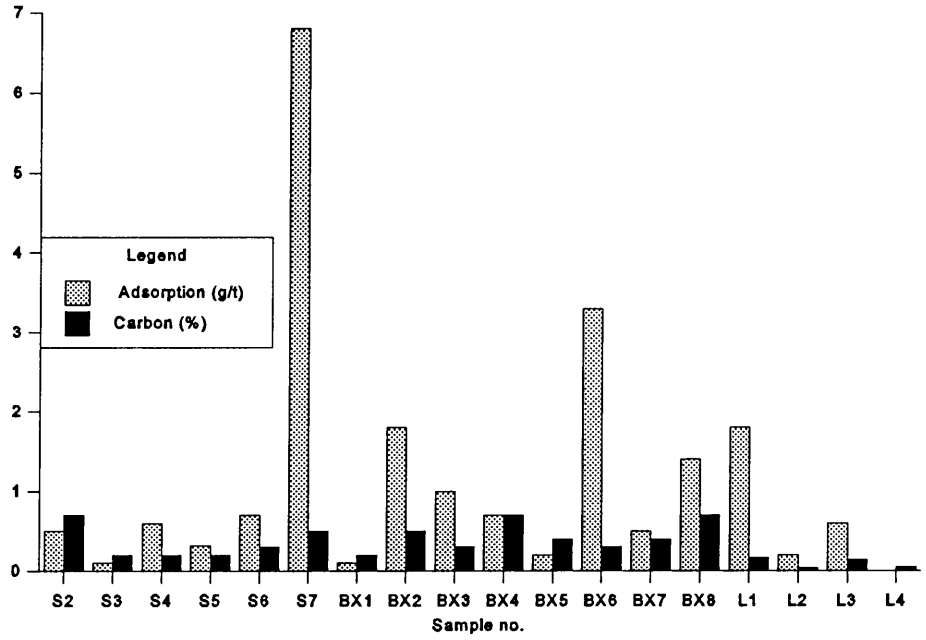

Figure 24 Gold adsorption compared with organic carbon content

The gold adsorption is compared to the bulk chemistry by using Spearman rank correlation coefficients (Table 16). According to the correlation coefficients there seems to be no correlation between the major elements and trace elements on the one hand, and gold adsorption on the other. This suggests that the bulk chemistry does not have a major influence on gold adsorption. Neither does the matrix of correlation between gold adsorption and the normative minerals indicate that an obvious correlation exists between mineralogy and gold adsorption (Table 17), but there seems to be a tendency that high gold adsorption values are preferentially related to high percentages of FeO (corrected for pyrite) + MgO + Al_2O_3 (corrected for muscovite). However, the opposite is not necessarily true (Fig 25). These corrections are as follows:

1.(a) Pyrite correction: Subtract 1.35 x %S from Fe_2O_3

(b) Convert remaining Fe_2O_3 to FeO: FeO = 0.90 x $\%Fe_2O_3$

2. Muscovite correction: Subtract 3.25 x $\%K_2O$ from Al_2O_3

If this tendency should indeed exist, it could imply that the less stable phyllosilicates were partially decomposed in the strongly alkaline cyanide solutions, and that gold could be co-precipitating with colloidal $Mg(OH)_2$ and $Fe(OH)_3$ formed during the reaction. It is known that hydrated colloidal iron oxides adsorb gold from solution (Krendelev, Zhmodik and Mironov, 1978; Enzweiler and Joekes, 1990). To examine this possibility mass balances were determined.

TABLE 16 Spearman rank correlation coefficients between the major and trace elements and gold adsorption.

Trace element	Correlation	Major element	Correlation
Zn	0.09	SiO_2	-0.23
Cu	0.00	TiO_2	0.14
Ni	0.15	Al_2O_3	0.18
Ga	0.22	Fe_2O3	0.16
Mo	-0.12	MnO	0.14
Nb	0.13	MgO	0.09
Zr	-0.14	CaO	-0.18
Y	-0.37	Na_2O	-0.14
Sr	-0.13	K2O	0.18
Rb	0.18	P_2O_5	0.09
U	-0.16	Cr_2O_3	-0.09
Th	-0.16	NiO	-0.21
Pb	-0.20		
Co	-0.09		
Cr	-0.08		
V	0.25		
Ba	0.09		
Sc	0.30		
S	-0.26		
As	-0.09		

TABLE 17 Spearman rank correlation coefficients between normative mineralogy and gold adsorption

	Adsorption	Pyrite	Paragonite	Muscovite	Fe-Chlorite	Mg-Chlorite	Pyrophyllite	Rutile	Quartz
Adsorption	1.00	-0.24	-0.14	0.18	0.22	-0.01	0.08	0.17	-0.20

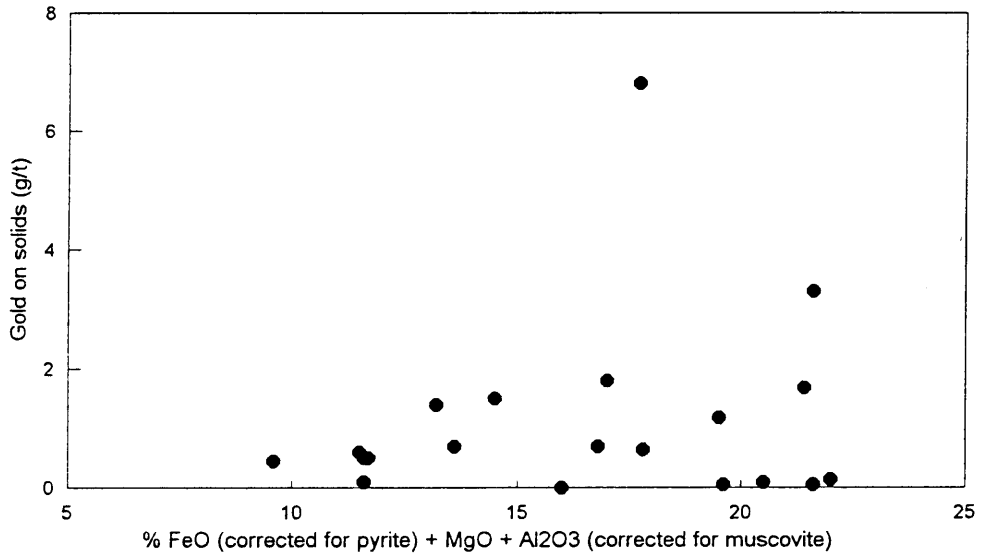

Figure 25 FeO (corrected for pyrite) + MgO + Al_2O_3 (corrected for muscovite) *v.* gold on the solids.

3.3 Mass balance determinations

The mass balance determinations involved experiments whereby 70g of powdered shale (90% < 75μ) were mixed by means of a magnetic stirrer, with 70ml of a 30g Au/ton gold cyanide solution (in a 1:1 solid/liquid-ratio), for different time intervals. The intervals were 15, 30, 60 and 180 minutes respectively. After a specific time interval the experiment was stopped and the solids were separated from the solution by using a Buchner vacuum filter flask. The solids were washed with 70 ml of deionised water before their gold contents were determined. XRF analysis was also done on a representative portion of the remaining solids from each experiment to see if any changes in the bulk chemistry took place. However, the XRF analyses were not sensitive enough to detect any change in the bulk chemistry. By using atomic absorption spectrometry the gold, iron, magnesium, aluminium and silica concentrations were determined in the spent cyanide- and washing solutions. These tests were only done on samples BX1, BX5, BX6, and BX8.

BX1 contained a high amount of rectorite and as soon as the sample was added to the gold cyanide solution a thick pulp was formed which made it virtually impossible to separate the solids from the liquid. It is therefore evident that rectorite indeed behaved like a smectitic mineral, similar to montmorillonite. It is not clear whether the sample selectively adsorbed gold from the cyanide solution as any possible adsorption was totally overshadowed by the absorption of the solution.

Samples BX5, BX6 and BX8 did not contain significant amounts of rectorite and the separation of the solids from the liquid took about three minutes. One may therefore assume that any chemical reactions stopped within about three minutes after stopping the experiment. Table 18 and Figure 26.a-c show the results of the change in pH, gold in solution and gold on solids from these experiments.

TABLE 18 Results of mass balance experiments.

Sample	Time(min.)	pH	Au g/ton in solution	Au g /ton in wash solution	Au g/ton on solids (assay)
Standard	0	12.03	29.92	-	1.00
BX5-0	15	11.11	26.70	2.85	2.62
BX5-1	30	10.93	27.19	4.68	2.62
BX5-2	60	10.97	26.40	3.27	2.75
BX5-3	180	10.25	25.69	3.85	4.28
Standard	0	12.03	29.92	-	0.10
BX6-0	15	10.97	21.01	3.25	5.75
BX6-1	30	11.08	19.13	3.54	6.22
BX6-2	60	10.84	17.86	3.79	7.45
BX6-3	180	10.20	17.05	1.69	8.45
Standard	0	12.03	29.92	-	0.45
BX8-0	15	9.96	19.72	4.46	7.02
BX8-1	30	10.18	20.86	4.47	8.72
BX8-2	60	10.15	19.31	3.78	6.18
BX8-3	180	9.75	18.19	4.80	8.32

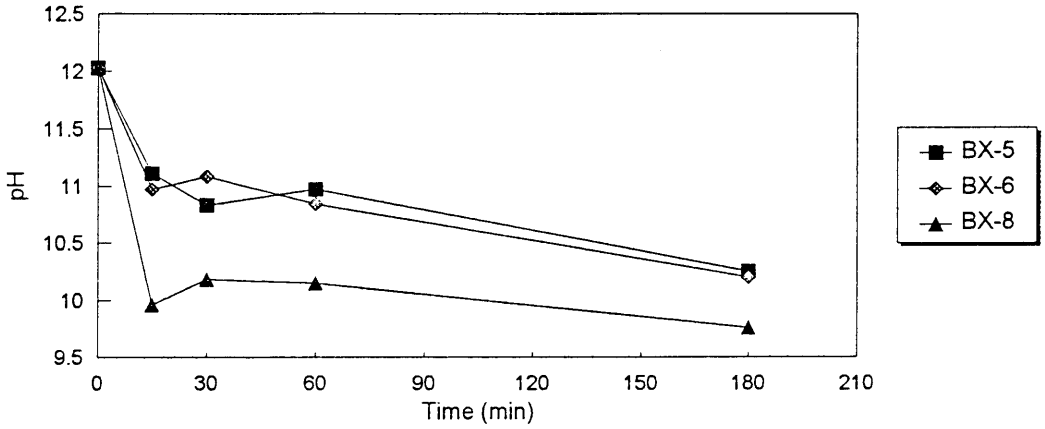

a) pH of solutions.

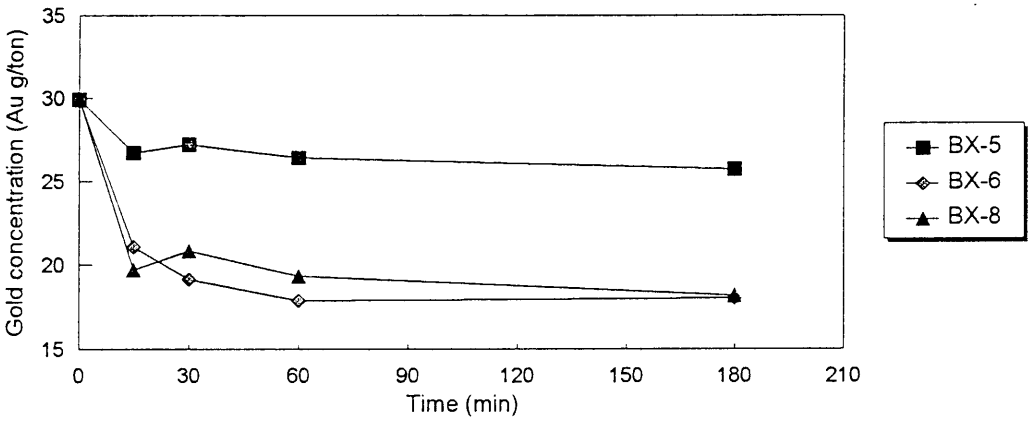

b) Gold in solution.

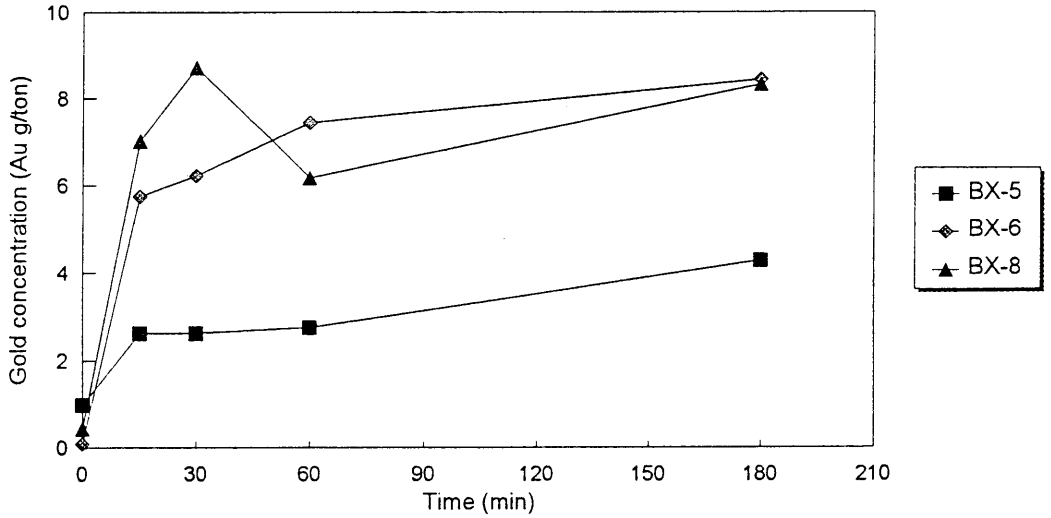

c) Gold concentration on solids

Figure 26 Results of mass balance experiments.

The results show that there is a decrease in pH over time and that the biggest pH drop occurs within the first 15 minutes, producing an exponential pattern for pH decrease (Fig. 26.a). This drop in pH might lead to gold precipitation.

Phyllosilicates such as pyrophyllite, muscovite and chlorite that are decomposed in the strongly alkaline solution may be responsible for this drop in pH. As a result $Fe(OH)_3$ and, $Mg(OH)_2$ would form and might lead to the adsorption of gold. Table 19 shows that the solutions contain considerable amounts of *Al* and *Si*, but no *Mg* and *Fe*. The *Mg* and *Fe* liberated by the decomposition of the phyllosilicates therefore precipitate immediately on the surface of the shale particles in the pulp. A combination of the data in Tables 18 and 19 (Fig 27) shows that a weak positive trend exists between the amount of $Si + Al$ in solution and the amount of gold adsorbed on the solids. BX8 contains about 85% of normative phyllosilicates (and less than 1% chlorite), followed by BX6 (66% phyllosilicates, 9% chlorite) and BX5 (64% phyllosilicates, 17% chlorite). Broadly speaking this listed sequence is in agreement with the drop in pH of the solutions and the amount of gold adsorbed on the solids (Fig. 26). It therefore appears as if pyrophyllite and muscovite may be contributing factors in the adsorption of gold from solutions.

The major decrease in gold occurs within the first 15 to 30 minutes and although the drop in pH and in gold concentration of the solutions vary sympathetically (Fig. 26), it is not a linear relationship, as the trends for BX6 and BX8 are inverted in Fig. 26(a) with respect to Fig. 26(b). A direct relationship between the lowering in pH of the solution and the propensity to adsorb gold therefore does not exist.

TABLE 19 Elements in solution.

Experiment	Mg (ppm)	Fe (ppm)	Al (ppm)	Si (ppm)
BX5-0	-	-	15	21
BX5-1	-	-	12	28
BX5-2	-	-	16	31
BX5-3	-	-	17	24
BX6-0	-	-	8	30
BX6-1	-	-	11	34
BX6-2	-	-	11	31
BX6-3	-	-	12	36
BX8-0	-	-	10	15
BX8-1	-	-	27	44
BX8-2	-	-	15	29
BX8-3	-	-	11	20

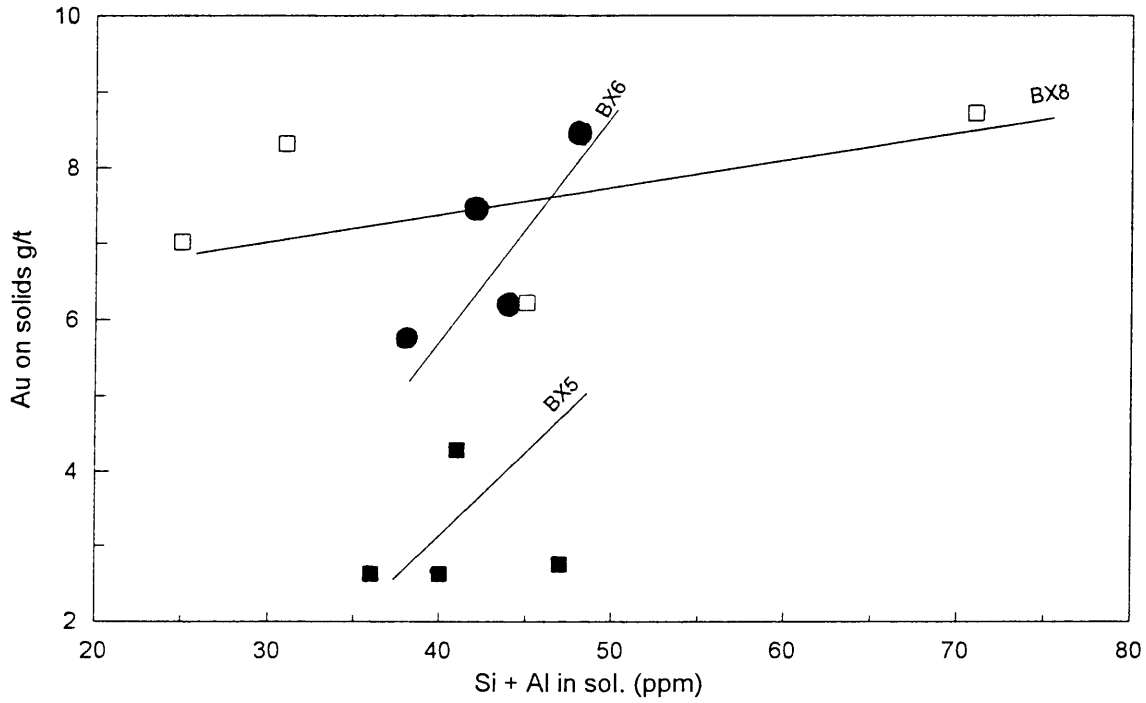

Figure 27. Al + Si in solution *v.* gold on the solids.

The mass balance calculation was done by comparing the gold content of the various solutions before and after each experiment:

Before the experiment: $\text{Gold}_{\text{total}} = \text{Gold}_{\text{initial solution}} + \text{Gold}_{\text{initial grade}}$

After the experiment: $\text{Gold}_{\text{total}} = \text{Gold}_{\text{final grade}} + \text{Gold}_{\text{final solution}} + \text{Gold}_{\text{washing solution}}$

$$\textit{Recovery} = \frac{\textit{Total gold after experiment}}{\textit{Total gold before experiment}} \times 100\%$$

The gold in the washing solution represents the absorbed gold that has been removed during the washing process. It is important to note that roughly the same amount of gold was absorbed on the shales for the different time intervals. This shows that after about 15 minutes no more gold absorption took place. A mass balance value of 100 ± 10% would indicate that no gold has been lost or gained. The mass balance results (Table 20) show that no precipitation of gold occurred on the sides of the container but that gold was adsorbed on phases in the solids.

TABLE 20 Mass balance calculation showing the recovery of gold.

Experiment	Initial solution (ppm)	Final solution (ppm)	Initial grade (ppm)	Final grade (ppm)	Gold in washing sol. (ppm)	Recovery (%)
BX5-0	29.92	26.7	1.00	2.62	4.07	108.00
BX5-1	29.92	27.19	1.00	2.62	6.68	118.03
BX5-2	29.92	26.4	1.00	2.75	4.67	109.38
BX5-3	29.92	25.69	1.00	4.28	5.50	114.72
BX6-0	29.92	21.09	0.10	5.75	4.64	104.87
BX6-1	29.92	19.13	0.10	6.22	5.05	101.29
BX6-2	29.92	17.86	0.10	7.45	5.41	102.35
BX6-3	29.92	18.04	0.10	8.45	5.65	107.06
BX8-0	29.92	19.72	0.45	7.02	6.37	109.03
BX8-1	29.92	20.86	0.45	8.72	6.38	118.43
BX8-2	29.92	19.31	0.45	6.18	5.40	101.71
BX8-3	29.92	18.19	0.45	8.32	6.86	109.87

3.4 Gold adsorption on polished sections

Carbonaceous particles were located in the polished sections and marked by means of a diamond marker. The polished sections were then brought into contact with a 100g Au/ton cyanide solution for 48 hours. After they have been taken out of the gold cyanide solution the polished sections were washed with distilled water. A Scanning Electron Microscope was then used to detect any adsorbed gold on the particles. No gold was however detected. This was probably because the SEM is not sensitive enough to detect gold in concentrations lower than about 500 g Au/ton.

3.5 Gold adsorption on coaly material and activated carbon

3.5.1 Adsorption on peat, lignite and coal

Coal of varying rank with low ash contents (Boshoff *et al.*, 1991) were collected from the CSIR. The aim of these experiments was to correlate the rank of carbonaceous material to its ability to adsorb gold from gold cyanide solutions. In these experiments powdered coal of varying rank were submersed in a 22 g Au/ton cyanide solution in a 1:1 solid/liquid ratio for 15 minutes. The solids were then separated from the cyanide solution by means of a Buchner flask and a vacuum pump. The gold concentration in the depleted cyanide solution was then determined by means of atomic absorption spectroscopy. Table 21 lists the gold adsorption results for the coaly material and activated carbon whereas Figure 28 is a graphical representation.

TABLE 21 Results of gold adsorption on coaly material.

Sample nr.	Rank (Rm %)	Gold conc. (g/ton) (Stock solution)	Gold conc. (g/ton) (Depleted solution)	Adsorption (%)
C1 (Peat)	0.20	22.00	7.15	67.50
C2(Lignite)	0.30	22.00	4.10	81.36
C3	0.59	22.00	14.10	35.91
C4	0.60	22.00	15.39	30.05
C5	0.60	22.00	13.90	36.82
C6	0.65	22.00	15.43	29.86
C7	0.67	22.00	17.27	21.50
C8	0.68	22.00	15.39	30.05
C9	0.69	22.00	17.12	22.18
C10	0.70	22.00	10.18	53.73
C11	0.94	22.00	18.90	14.09
C12	1.04	22.00	20.50	6.82
C13	1.43	22.00	14.80	32.73
C14	1.60	22.00	16.80	23.64
C15	2.01	22.00	3.06	86.09
C16	2.37	22.00	0.75	96.59
C17	2.38	22.00	1.05	95.23
C18	2.53	22.00	0.13	99.41
C19	2.69	22.00	1.20	94.55
C20	2.70	22.00	0.08	99.64

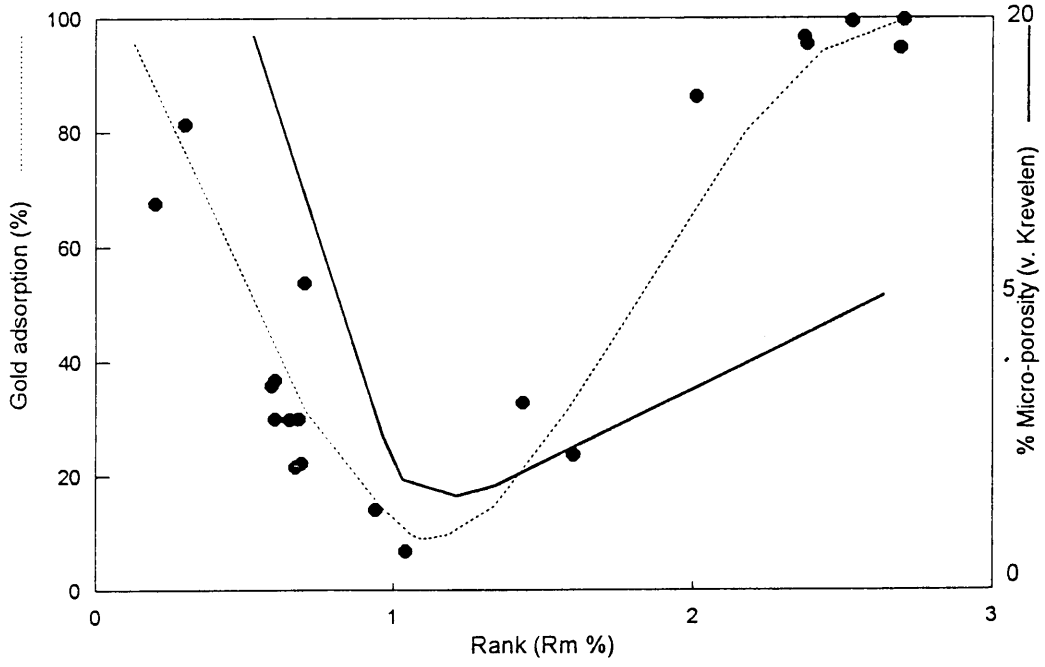

Figure 28 Results of gold adsorption on coal of varying rank. Note the minimum gold adsorption at a rank of about 1.2% R_m.

The results show that the gold adsorption has high values for peat and lignite and for semi-anthracite and anthracite. The lowest values are for the medium volatile bituminous coals (R_m = 1.04%). In Fig. 28 a second graph of the variation in microporosity with coal rank according to van Krevelen (1961), is also shown. In the case of low rank coals a fairly close similarity between the graphs of microporosity and gold adsorption capacity is evident, but in the case of higher rank coals (above 1.0% R_m) the two graphs deviate from each other, although the trend remains the same. The adsorption capacity is therefore not only determined by the microporosity (and hence the internal surface area which may vary between *c*a. 30 and 300m^2/g) of the coal, but perhaps even to a greater extent by the "active sites" on the internal surface. Anthracites seem to have more "active sites" in spite of their lower microporosity compared to low rank coal.

3.5.2 Gold adsorption on anthracite compared with activated carbon

The adsorption of gold on anthracite within a specific time interval was compared with that of activated carbon. Powdered coal (C20) and activated carbon were immersed in a 30 g Au/ton cyanide solution at a 1:2 solid/liquid ratio for 15 minutes. The concentration of the depleted gold-cyanide solution was then determined by means of atomic adsorption spectroscopy. The results are given in Table 22.

The results show that activated carbon adsorbs about twice as much gold as anthracite in the specific time interval. Figure 29 shows the surface of a grain of the activated carbon while the surface of one of the coal particles is shown in Figure 30.

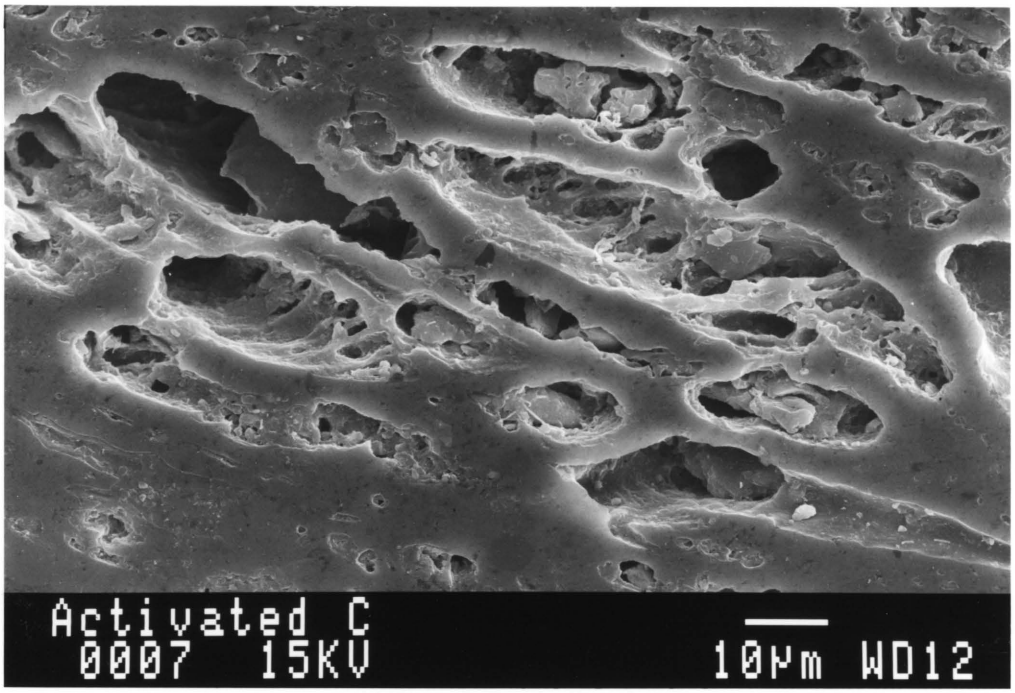

Figure 29 Electron-photomicrograph of the surface of activated carbon. Note the extremely porous nature of the particle.

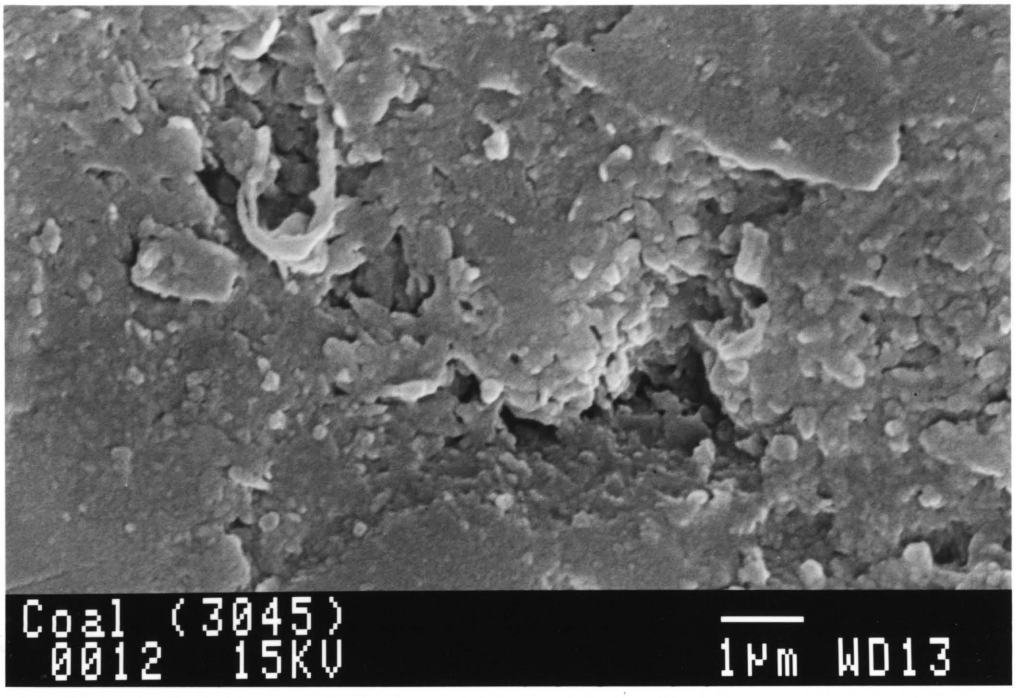

Figure 30 Electron -photomicrograph of a grain of anthracite. Note the much less porous nature when compared to activated carbon (Fig. 29).

3.5.3 Gold adsorption by anthracite at low solid/liquid ratios

The aim of this experiment was to determine whether a small amount of carbon (similar to the average amount in the shales) could adsorb a significant amount of gold. For this experiment 0.5g of powdered coal (C20) was immersed in 50 ml of a 22 g Au/ton cyanide solution for 30 min. The gold concentration of the remaining solution was determined by means of atomic absorption spectrometry. The results (Table 23) show that this low amount of anthracite was able to adsorb 5.5g Au/ton (or 25%) of the gold in the cyanide solution. This suggests that if a shale contained 1% carbonaceous matter with adsorption properties similar to those of anthracite used in this experiment, and if all this carbonaceous matter was in contact with the gold cyanide solution, it would adsorb a similar amount of gold.

TABLE 22 Results of gold adsorption on anthracite and activated carbon.

	Gold concentration in soln. before (Au g/ton)	**Gold concentration in soln. after (Au g/ton)**	**Adsorption (%)**
Activated carbon	30.04	1.4	95.34
Coal (C20)	30.04	12.45	58.56

TABLE 23 Result of gold adsorption experiment with a low solid/liquid ratio.

	Concentration in soln. before (Au g/ton)	**Concentration in soln. after (Au g/ton)**	**Adsorption (%)**
C20	22.00	16.50	25.00

4. DISCUSSION

From previous work and work done in this study, it is evident that there are two factors which may influence gold adsorption *viz.* the mineralogy of the shales and the finely dispersed carbonaceous matter.

4.1 Influence of mineralogy on gold adsorption

Krendelev *et al.* (1978) used the radioisotope ^{195}Au to examine the sorption by layer silicates (vermiculite, montmorillonite, illite, and kaolinite) as well as by the iron hydroxide goethite. They used gold cyanide solutions of pH 1.6, 6.2 and 10.2 and their results showed that gold was adsorbed mainly from the acidic and neutral solutions with vermiculite having the highest specific gold uptake. Vermiculite also had the highest cation-exchange capacity. Goethite had the highest total sorption and the largest specific surface which is in agreement with work done by Enzweiler and Joekes (1990,1991) who showed that colloidal iron oxides do indeed adsorb gold from solutions. At high pH levels the gold remained in solution and no significant gold adsorption by the minerals took place.

Logan (1986) did gold adsorption experiments with illite, chlorite, sericite, phlogopite, kaolinite, and pyrophyllite but detected no gold adsorption by any of these minerals under conditions approximating those in a reduction plant.

The results obtained from the gold adsorption experiments in this study suggest that the adsorption of gold onto mineral phases does not take place but that the decomposition of phyllosilicates in the highly alkaline solutions cause gold to co-precipitate with phases such as $Mg(OH)_2$ and $Fe(OH)_3$.

4.2 Influence of carbonaceous matter

To put the influence of the carbonaceous particles on gold adsorption into perspective it is necessary to understand which properties of activated carbon influences its ability to adsorb gold. Activated carbon has been used for some time for the recovery of gold from cyanide leach pulps but the mechanism by which the carbon adsorbs gold is still uncertain. There are currently two schools of thought regarding the adsorption mechanism:

i) Aurocyanide is adsorbed as an ion pair of the form $M^{n+}[Au(CN)^-_2]n$;

ii) Aurocyanide is adsorbed with the decomposition of $Au(CN)_2^-$ to AuCN.

Adams (1991) did Fourier-transform infrared spectrophotometric studies of adsorbed aurocyanide species on activated carbon. His results indicate that the aurocyanide species adsorb onto activated carbon without undergoing chemical change. However, no distinction could be made between adsorbed aurocyanide in the form of $M^{n+}[Au(CN)_2^-]n$ ion pairs and $Au(CN)^-_2$.

The adsorption property of activated carbon is thought to be achieved by three properties that are common to all activated carbons *viz.* a large specific surface area, a partially oxidised surface, and a charred (carbonized) organic substrate. The large surface area is necessary because the surface provides the sites on which adsorbed materials reside. Charring and partial oxidation are believed to give rise to the chemical properties of activated carbon.

Miller and Sibrell (1991) used activated carbon, carbon blacks, graphites and diamond during research on the nature of gold adsorption by activated carbon from cyanide solutions. They determined the surface area, pore volume distribution, microcrystallite size, functional group content, and gold adsorption of the various carbons. They found that activated carbon generally had the highest surface area, followed by carbon blacks, graphite and diamond. It was shown that there is a good correlation between gold adsorption and surface area and they found that the porosities of the samples generally followed the same trend as surface area, but with some significant differences. The pore structure

in activated carbon is caused by the misalignment of microcrystallites, and as such tends to favour very small pores. In carbon blacks, aggregates are formed from the much smaller primary particles, resulting in a more open structure, though still with some porosity. Graphite have much larger crystallites, resulting in large faults and pore spaces in their structure. They suggested that activated carbons are microporous, carbon blacks mesoporous; and graphites, macroporous.

They used X-ray diffraction to determine the crystalline structure and showed that graphite has a well defined crystalline structure but due to much greater disorder, and therefore smaller microcrystallite sizes, activated carbon showed a less developed crystalline structure. Carbon blacks appeared to have a similar crystallinity as activated carbon. Graphite had the largest crystallites, followed by activated carbon and carbon blacks. The results of gold adsorption experiments showed that there is a fair correlation between microcrystallite size and gold adsorption which suggests that microcrystallite size is a important factor in gold adsorption by carbon.

They concluded that one of the most important points brought out by their experimental results is that all of the samples with a graphitic structure, regardless of porosity, adsorbed gold to some extent. Diamond did not adsorb gold despite the presence of functional groups in amounts equivalent to some of the graphite samples. They suggest that the chemical bonding associated with the graphite structure plays a major role in gold adsorption because of the availability of electrons for bonding which are not available in the diamond crystal form. Their experimental results indicate that acidic functional groups do not play a significant role in gold adsorption. They also suggest that the strong correlation between structural properties, such as surface area and microcrystallite size, and gold adsorption indicates that these factors strongly influence the capacity for gold adsorption but that these structural features may only be prerequisites to facilitate contact of the solution with the graphitic structure, where some of the non-site-specific chemical bond is formed. They alternatively suggested that the

energy of adsorption may be increased at defects in the crystal structure, leading to site-specific adsorption in those areas.

Ibrado and Fuerstenau (1992) used different carbonaceous materials for gold adsorption experiments which included coal (lignite, bituminous coal and anthracite) and activated carbon. Their experiments indicate that the extent of gold adsorption is roughly a function of the rank of the carbonaceous adsorbent. They concluded that aside from a large surface area, the most important property of activated carbon with respect to gold cyanide adsorption is its highly graphitic structure (aromaticity). They suggest that oxygen and oxygen-containing functional groups play a significantly smaller role in gold adsorption than is generally believed because their results show that oxygen tends to depress gold adsorption. They further suggest that gold cyanide resides on the plate faces of the graphite crystallites upon adsorption on activated carbon.

In the current study the results obtained from the gold adsorption experiments with coal show that there is a minimum gold adsorption for coal with a rank of about 1.2 % R_m. At low rank stages gold adsorption of about 70% is reached and at anthracite rank stages 98%. As discussed in Section 3.5, the properties of porosity, inherent surface area and moisture of coal vary with the rank. They decrease with increase in rank from the brown coal stage to that of medium volatile bituminous A coals where a minimum is reached at about 1.6% R_m and 20% volatile matter. These properties then increase with increase in rank to the anthracite stage. The results of this experiment are broadly in agreement with those obtained by Ibrado and Fuerstenau (1992).

5. SUMMARY AND CONCLUSIONS

The present study was done to determine which characteristics of shale from bands within and overlying Beatrix Reef are responsible for its ability to adsorb gold from cyanide solutions. It was found that the shales are low grade metamorphic rocks with the mineralogy (pyrophyllite, muscovite, chlorite, chloritoid and rectorite) suggesting that it had undergone low grade greenshist facies metamorphism. Two types of carbonaceous particles resembling kerogen were observed in these shales. The one type is roundish and the other filamentous. Reflectivity measurements made on the carbonaceous particles indicate that they fall in the anthracite range.

Gold adsorption tests were undertaken on samples of these shales. The tests showed that the various samples have different propensities to adsorb gold, and that no obvious correlation exists between the carbon content of the shale and its ability to adsorb gold. Gold adsorption experiments showed that there is a drop in pH over time which is caused by phyllosilicates being dissolved in the highly alkaline solutions. Gold adsorption tests were also done on coal with varying rank. The results showed that coal with the highest rank (anthracite) had the highest gold adsorbing ability.

Based on the results from the experiments in this study the following conclusions are drawn:

i) The absorption of gold bearing-solutions is mainly due to rectorite. It is however doubtful whether rectorite would play a major role in a plant situation as it would be saturated with water from the underground workings and milling operations at the time it reaches the gold extraction plant.

ii) The mineralogy of the shales does not seem to have a major influence on the gold adsorption properties of a shale. However, results suggest that some gold loss can be caused as a result of the co-precipitation of gold with $Mg(OH)_2$ and $Fe(OH)_3$.

iii) The carbonaceous particles in the shales resemble a high ranking coal (anthracite), that has a relatively high microporosity and internal surface area and it is concluded that the carbonaceous particles probably adsorb gold in a similar

way and to the same extent as anthracite. Because of the different structures of the two types of carbonaceous particles it is possible that they may have different gold adsorption properties. The carbonaceous particles in the shale close to basic intrusions may be more "active" as a result of the heat of the intrusions. The extent of liberation of the carbonaceous particles during milling of the shale determines how many of the particles are exposed to the gold cyanide solution. This may explain the lack of correlation between gold adsorption and the carbon content of the shales. The filling of the internal pores of the carbonaceous particles by phases such as pyrite probably also lowers the gold adsorption capacity of such particles.

iv) Theoretically, the maximum potential of a shale to adsorb gold could be indicated by the carbon concentration and to a lesser extent by the concentration of iron-rich phyllosilicates. If all the carbonaceous particles in a shale are liberated during milling, and very little of the internal pores are filled by minerals such as pyrite, then it should adsorb a maximum amount of gold.

6. ACKNOWLEDGEMENTS

I wish to express my gratitude to the following persons and institutions without whom this project would not have been possible:

1. Gencor for providing the shale samples, performance of gold adsorption experiments and financial support. I would like to single out Dr. D.H. Holtum and Mr. P.R. Bailey for their keen interest and support with this project.
2. Messrs. G. Briggs, R. van Reysen and the personnel of the geology departments at Beatrix and Leslie Gold Mines in aiding with the collection of samples.
3. The CSIR for reflectivity measurements and the provision of coal samples.
4. ISCOR for atomic absorption spectrometry analyses of cyanide solutions and the provision of coal samples.
5. The FRD for financial support.
6. Dr. M. Sharpe for XRF analyses and Sabina Verryn for XRD analyses.
7. Prof. C.P. Jansen van Vuuren for valuable discussions and the use of his facilities.
8. Prof. C.P. Snyman for his ideas, guidance and patience.

Last but not least, thanks to my wife Alta, for all her support during the period of this study.

6. REFERENCES

ABOTSI, G.M.K. AND OSSEO-ASARE, K. (1986). Surface chemistry of carbonaceous gold ores I. Characterization of the carbonaceous matter and adsorption behaviour in aurocyanide solutions. *Intl. J. Min. Processing.*, **18**, 217-236.

ABOTSI, G. M. K., AND OSSEO-ASARE, K. (1987). Surface chemistry of carbonaceous gold ores, II. Effect of organic additives on gold adsorption from cyanide solution. *Intl. J. Min. Processing*, **21**, 225-239.

ADAMS, M. D. (1991). Fourier-transform infrared spectrophotometric study of adsorbed aurocyanide species on activated carbon. *Hydrometallurgy*, **31**, 111-120.

ADAMS, M. D., FRIEDL, J. AND WAGNER, F.E. (1991). The mechanism of adsorption of $Au(CN)_4^-$ onto activated carbon. *Hydrometallurgy*, **31**, 265-275.

BAILEY, S. W., 1988. Chlorites: structure and crystal chemistry, In: BAILEY, S. W., (Ed.), *Reviews in mineralogy* ,**19**, *Hydrous phyllosilicates.*

BOSHOFF, H.P, BERGH. C.E. AND KRUSZEWSKA, K.J. (1991). Analysis of coal product samples of producing South African collieries. *Enertek. Bull.*, **105**.

BUSECK, P. R., AND HUANG BO-JUN (1985). Conversion of carbonaceous material to graphite during metamorphism. *Geochim. Cosmochim. Acta* **49**, 2003-2016.

CLAASSEN, R., 1991. Microbiological oxidation of sulphide minerals from Agnes, New Consort and Sheba goldmines. *Msc. thesis*, Univ. Pretoria.

CRYSSOULIS, S. L., STOWE, K. G. AND REICH, F. (1992). Characterization of composition of mineral surfaces by laser-probe microanalysis. *Trans. Instn Min. Metall. (Sect. C: Mineral Process. Extr. Metall.)*, **101**.

DAIRA DUBA, AND WILLIAMS-JONES, A. E. (1983). The application of illite crystallinity, organic matter reflectance, and isotopic techniques to mineral exploration: A case study in Southwestern Gaspe, Quebec. *Econ. Geol.*, **78**, 1350-1363.

DE WAAL, S. A. (1982). A literature survey of the metallurgical aspects of minerals in Witwatersrand gold ores. *Council for Mineral Technologuy, Report M37.*

EBERL, D. AND HOWES, J. (1977). The hydrothermal transformation of sodium and potassium smectite into mixed-layer clay. *Clays and Clay minerals*, **25**, 215-227.

ENZWEILER, J. AND JOEKES, I. (1990). Adsorption of colloidal gold on colloidal iron oxides. *J. Geochem. Explor.*, **40**, 133-142.

ENZWEILER, J. AND JOEKES, I. (1991). Hetero- and homocoagulation of colloidal gold and iron oxides. *J. Colloid Interface Sci.*, **150**, 559-566.

EVANS, B. W. AND GUGGENHEIM, S. (1988). Talc, Pyrophyllite, and related minerals, In: Bailey, S. W. (Ed.) Reviews in mineralogy,**19**, *Hydrous phyllosilicates.*

FEATHER, C. E. AND KOEN, G. M. (1975). The mineralogy of the Witwatersrand reefs. *Minerals Sci. Engng.*, **7**, 189-204.

FRIDMAN, I.D. AND SAVARI, E. E. (1983). A study of the sorption properties of the carbon-containing constituents of gold-arsenic ores. *Tsvetnye Metally/Non-Ferrous metals,* **26** no **4**, 115-137.

GOULD , D. G. (1991). Laboratory procedure for quantifying gold adsorption onto shales. *GPR Report,* **91/122**.

GUIDOTTI, C. V. (1984). Micas, In: BAILEY, S. W. (Ed.), Reviews in mineralogy, 13, *Micas in metamorphic rocks.*

GUY, W. J. (1981). Treatment of refractory gold ores containing carbonaceous material and sulfides. In: SCHLITT, W. J., LARSON, W. C. AND HISKY, J. B. (Eds.), *Gold and silver leaching, recovery and economics.* Proc. 110th AIME meeting, Chicago, Illinois, **Feb22-26,1981**.

HALLBAUER, D. K., AND VAN WARMELO, K . T. (1974). Fossilized plants in thucholite from Precambrian rocks of the Witwatersand, South Africa. *Precambrian Res.*, **1**, 199-212.

HALLBAUER, D. K. (1986). The mineralogy and geochemistry of Witwatersrand pyrite, gold, uranium, and carbonaceous matter. 731-752. In:ANHAEUSSER, C. R. AND MASKE, S. (Eds.), *Mineral Deposits of Southern Africa,* 1. Geol. Soc. S. Afr., Johannesburg, 1020 pp.

HALLBAUER, D. K. (1975). The plant origen of the Witwatersrand 'carbon'. *Minerals Sci. Engng.,* 7, 111-136.

HAUSEN, D. M., AND BUCHNAM, C. H. (1984). Study of preg-robbing in the cyanidation of carbonaceous gold ores from Carlin, Nevada. *ICAM 84.*

HOEFS, J., AND SCHIDLOWSKI, M. (1967). Carbon isotope composition of carbonaceous matter from the Precambrian of the Witwatersrand System. *Nature,* **155**, 1096-1097.

HOLTUM, D. A. (1990). Carbon-in-leach (CIL) and gold adsorption onto shale. *GPR Report* **90/109**.

IBRADO, A. S., AND FUERSTENAU, D. W. (1992). Effect of the structure of carbon adsorbents on the adsorption of gold cyanide. *Hydromettalurgy,* **30,** 243-256.

KRENDELEV, F. P., ZHMODIK, S.M., AND MIRONOV, A.G. (1978). A ^{195}Au study of the sorption of gold by natural layer silicates and iron hydroxides. *Geochim. Int.,* **15**, 156-162.

LOGAN, C. T. (1986). A mineralogical investigation of potential gold-sorbing minerals and shales. *Mintek report no M294.*

MILLER, J. D., AND SIBRELL P. L. (1991). The nature of gold adsorption from cyanide solutions by carbon. *EPD Congress '91,* 647-663.

OSSEO-ASARE, K., AFENYA, P. M. AND ABOTSI, G. M. K. (1984). Carbonaceous matter in gold ores: Isolation, characterization and adsorption behavior in aurocyanide solutions. Eds. *Kudryk et. al. Met. Soc. AIME,* 125-144.

PHILLIPS, G. N. (1988). Widespread fluid infiltration during metamorphism of the Witwatersrand goldfields: generation of chloritoid and pyrophyllite. *J. metamorphic Geol.,***6**, 311-332.

PHILLIPS, G. N., AND LAW, J. D. M. (1992). Metamorphic petrology of the Witewatersrand Supergroup. *Econ. Geol. Res. Unit. Univ Witwatersrand, Johannesburg.* Inf. Circ. , **248**, 43pp.

PRICE, L. C. (1983). Geologic time as a parameter in organic metamorphism and vitrinite reflectance as an absolute paleogeothermometer. J. Petrol. Geol. **6**(1), 5-38.

RIBBE, P. H. (1982). Chloritoid. In: Ribbe, H. R. (Ed.), *Reviews in mineralogy*, **5**, *Orthosilicates*, second ed.,

SNYMAN, C. P. (1965). Possible biogenetic structures in Witwatersrand Thucholite. *Trans. Geol. Soc. S. Afr.*, **63**, 225-235.

SOUTH AFRICAN COMMITEE FOR STRATIGRAPHY (SACS) (1980). Stratigraphy of the Republic of South Africa, South West Africa/Namibia, and the Republics of Bophuthatswana, Transkei and Venda. *Handbk. geol. Surv. S. Afr.*, **8**, 690 pp.

STACH, E. MACKOWSKY, M. -TH., TEICHMULLER, M., TAYLOR, G. H., CHANDRA, D., TEICHMULLER, R. (1982). *Stach's Textbook of Coal Petrology.* Gebrüder Borntraeger, Berlin, Stuttgart. 535 pp.

TEICHMÜLLER, M., AND TEICHMÜLLER , R. (1979). Diagenesis of coal (coalification). In *Diagenesis in sediments and sedimentary rocks,* Vol. 1. LARSEN, G. AND CHILINGAR, G. V., (EDS.), *Developments in sedimentology,* **25A.** Elsevier, Amsterdam.

THOMPSON, A.B. (1970). A note on the kaolinite-pyrophyllite equilibrium. *Am. J. Sci.*, **268**, 454-458.

TING, F.C. (1978). New techniques for measuring maximum reflectance of vitrinite and dispersed vitrinite in sediments. *Fuel*, **57**, 717-721.

TWEEDIE, K. A. M., (1986). The discovery and exploration of Beisa and Beatrix gold and uranium mines in the southern extension of the Welkom Goldfield. In:ANHAEUSSER, C. R. AND MASKE, S. (Eds.), *Mineral Deposits of Southern Africa,* 1. Geol. Soc. S. Afr., Johannesburg, 1020 pp.

URBAN, M. R., URBAN, J., AND LLOYD, P. J. D. (1972). The adsorption of gold from cyanide solutions onto constituents of the reef, and its role in reducing the efficiency of the gold recovery process. *J. S. Afr. Inst. Min. Metall.*, **73**, 385-394.

VAN KREVELEN, R. (1961). *Coal.* Elsevier. Amsterdam.

VON RAHDEN, H. V. R., SLATEM, I. C., AND CORFIELD, A.A. (1994). Rectorite: A new phyllosilicate species in Witwatersrand paleoplacers. Its genesis and implications for the Gold-Mining Industry. *Process Mineralogy XII- Applications to Environment, Precious Metals, Mineral Benificiation, Pyrometallurgy, Coal and Refractories.* Edited by W. Petruk and A. R. Rule.

WALLMACH, T., AND MEYER, F. M. (1990). A petrogenetic grid for metamorphosed aluminous Witwatersrand shales. *S. Afr. J. Geol.*, **1**, 93-102.

WINKLER, G. F. (1976). *Petrogenesis of metamorphic rocks. Springer-Verlag , New York, 329pp.*

ZUMBERGE, E., ANNE, C., SIGLEO AND BARTHOLOMEW NAGY, (1978). Molecular and elemental analysises of the carbonaceous matter in the gold and uranium bearing Vaal Reef carbon seams, Witwatersrand Sequence. *Minerals Sci. Engng,* **10**, 223-246.

APPENDIX 1

Microprobe analyses of major silicate minerals

Muscovite									*Average*	*Std dev.*
SiO_2	45.46	45.17	46.82	46.25	47.85	49.17	55.31	57.57	49.20	4.38
CaO	0.10	0.83	0.13	0.09	0.05	0.41	0.66	0.15	0.30	0.28
Cr_2O_3	0.13	0.28	0.21	0.11	0.28	0.19	0.15	0.12	0.18	0.06
MgO	0.09	0.04	0.08	1.21	0.18	0.09	0.03	0.78	0.31	0.41
Al_2O_3	36.50	38.46	38.48	33.48	39.28	38.35	34.70	35.37	36.83	1.99
FeO	1.96	0.25	0.51	3.50	0.19	0.18	0.15	0.88	0.95	1.12
ZnO	0.03	0.00	0.02	0.00	0.00	0.01	0.00	0.01	0.01	0.01
Na_2O	0.57	1.33	0.70	0.86	0.12	0.47	0.17	0.49	0.59	0.36
MnO	0.00	0.00	0.00	0.00	0.00	0.00	0.00	0.00	0.00	0.00
K_2O	9.87	8.76	9.83	10.30	11.52	9.85	5.54	6.86	9.07	1.83
TiO_2	0.31	0.04	0.14	0.00	0.15	0.00	0.18	0.07	0.11	0.10
TOTAL	95.01	95.16	96.92	95.80	99.62	98.72	96.89	102.31	97.55	

Pyrophyllite							*Average*	*Std dev.*
SiO_2	66.98	67.56	68.50	67.33	66.54	68.50	67.57	0.73
CaO	0.10	0.08	0.08	0.09	0.10	0.06	0.08	0.02
Cr_2O_3	0.10	0.09	0.09	0.06	0.10	0.08	0.09	0.01
MgO	0.01	0.00	0.00	0.00	0.00	0.00	0.00	0.00
Al_2O_3	28.56	28.30	29.65	29.52	26.30	27.45	28.30	1.16
FeO	0.11	0.01	0.07	0.05	0.03	0.07	0.05	0.03
ZnO	0.00	0.03	0.04	0.00	0.08	0.01	0.03	0.03
Na_2O	0.32	0.00	0.00	0.00	0.00	0.00	0.05	0.12
MnO	0.05	0.00	0.01	0.01	0.00	0.00	0.01	0.02
K_2O	0.13	0.13	0.03	0.38	0.04	0.05	0.12	0.12
TiO_2	0.01	0.00	0.02	0.01	0.00	0.01	0.01	0.01
TOTAL	96.37	96.20	98.48	97.43	93.18	96.23	96.32	

Chloritoid				*Average*	*Std dev.*
SiO_2	24.81	25.03	24.23	24.69	0.34
CaO	0.04	0.01	0.03	0.03	0.01
Cr_2O_3	0.32	0.29	0.25	0.29	0.03
MgO	0.14	1.32	1.34	0.93	0.56
Al_2O_3	41.74	41.97	40.80	41.50	0.51
FeO	24.30	24.33	24.34	24.32	0.02
ZnO	0.01	0.02	0.07	0.03	0.02
Na_2O	0.14	0.00	0.00	0.05	0.07
MnO	1.20	1.22	1.14	1.18	0.03
K_2O	0.02	0.02	0.00	0.01	0.01
TiO_2	0.02	0.00	0.03	0.02	0.01
TOTAL	92.72	94.21	92.21	93.05	

Chlorite					*Average*	*Std dev.*
SiO_2	25.15	24.40	26.27	23.10	24.73	1.03
CaO	0.12	0.00	0.06	0.03	0.05	0.04
Cr_2O_3	0.19	0.15	0.20	0.28	0.21	0.04
MgO	13.42	13.59	8.39	7.99	10.85	2.38
Al_2O_3	27.81	27.35	29.61	30.87	28.91	1.26
FeO	24.47	25.65	27.34	30.62	27.02	2.07
ZnO	0.10	0.07	0.03	0.08	0.07	0.02
Na_2O	0.58	0.00	0.00	0.00	0.15	0.22
MnO	0.47	0.43	0.34	0.39	0.41	0.04
K_2O	0.14	0.05	0.61	0.80	0.40	0.28
TiO_2	0.05	0.02	0.03	0.00	0.03	0.02
TOTAL	92.51	91.71	92.87	94.16	92.83	

APPENDIX 2

Major and trace element data of shales from Leslie- (L1-L4) and Beatrix Gold Mines (S2-BX8)

	L1	L2	L3	L4	S2	S3	S4	S5	S6	S7	S8	S9	S10	S11	BX-1	BX-2	BX-3	BX-4	BX-5	BX-6	BX-7	BX-8
SiO_2	60.44	57.14	61.95	64.29	77.50	56.94	56.45	51.90	56.37	56.05	54.84	64.09	86.59	76.51	67.82	54.19	58.82	73.02	60.24	61.60	47.83	51.17
TiO_2	1.04	1.15	0.87	0.87	0.98	0.95	1.46	1.86	1.24	1.16	1.20	0.67	0.25	0.54	0.18	1.01	1.02	0.55	0.84	0.76	0.96	0.87
Al_2O_3	19.00	30.05	27.18	19.85	8.67	29.85	24.70	27.07	23.73	25.21	23.00	19.83	6.88	12.26	20.65	32.30	30.12	11.96	18.80	21.72	35.95	33.54
Fe_2O_3	7.13	1.57	0.58	4.38	5.58	1.37	4.38	4.76	5.05	5.15	7.92	4.27	2.04	3.47	0.82	0.36	0.40	5.85	6.93	4.70	0.31	0.58
MnO	0.28	0.20	0.05	0.24	0.02	0.00	0.03	0.01	0.04	0.05	0.06	0.04	0.03	0.05	0.00	0.00	0.00	0.07	0.08	0.02	0.00	0.00
MgO	3.83	0.82	0.20	2.68	0.79	0.62	1.36	1.13	1.67	1.60	2.51	2.48	0.72	1.31	0.42	0.18	0.12	2.80	3.63	1.67	0.15	0.20
CaO	0.37	0.54	0.17	0.27	0.04	0.34	0.10	0.08	0.08	0.10	0.00	0.07	0.05	0.02	1.55	0.19	0.23	0.13	0.17	0.12	0.17	0.17
Na_2O	0.59	0.70	0.63	0.64	0.24	0.50	0.40	0.45	0.42	0.30	0.38	0.44	0.15	0.26	1.76	0.50	0.44	0.24	0.39	0.57	0.66	0.63
K_2O	2.98	3.34	6.53	3.60	1.29	3.14	6.01	6.79	5.39	4.61	4.63	3.85	1.53	2.42	0.74	4.91	2.88	1.41	2.78	3.87	7.56	6.53
P_2O_5	0.20	0.23	0.02	0.20	0.02	0.03	0.10	0.06	0.06	0.06	0.04	0.00	0.02	0.03	0.02	0.03	0.04	0.04	0.00	0.00	0.03	0.02
Cr_2O_3	0.30	0.33	0.07	0.22	0.71	0.13	0.25	0.38	0.25	0.17	0.26	0.02	0.10	0.11	0.02	0.09	0.06	0.06	0.10	0.09	0.08	0.07
NiO	0.24	0.20	0.00	0.20	0.02	0.00	0.04	0.03	0.02	0.00	0.06	0.00	0.00	0.01	0.00	0.00	0.00	0.02	0.04	0.01	0.00	0.00
H_2O-	0.46	0.83	0.34	0.82	0.25	0.63	0.54	0.43	0.65	0.39	0.42	0.62	0.26	0.33	2.16	0.28	0.18	0.09	0.26	0.23	0.19	0.34
LOI	2.65	2.98	1.63	1.80	3.62	5.36	4.46	5.33	4.99	4.76	4.57	3.75	1.22	2.25	3.96	5.82	5.47	3.66	5.24	4.37	5.62	5.50
Total	99.51	100.08	100.22	100.06	99.73	99.86	100.28	100.28	99.96	99.61	99.89	100.13	99.84	99.57	100.10	99.86	99.78	99.90	99.50	99.73	99.51	99.62
Zn	123	23	17	70	148	22	56	69	67	79	113	69	33	57	14	8	7	97	122	71	6	8
Cu	33	16	32	35	49	15	81	84	39	36	515	34	16	27	29	22	12	98	32	41	16	16
Ni	307	50	905	220	210	49	318	306	226	217	515	219	73	164	31	124	53	243	306	272	48	64
Ga	22	35	27	24	5	34	22	24	26	28	30	23	6	12	29	41	33	10	21	27	40	34
Mo	5	4	3	5	13	3	12	12	10	7	3	4	9	7	3	3	3	4	4	3	3	3
Nb	16	19	9	16	17	18	24	31	25	21	23	15	6	12	6	13	13	11	15	14	16	15
Zr	178	333	148	206	1038	332	1440	1695	848	400	446	205	124	276	53	249	265	151	177	230	211	198
Y	57	26	15	21	33	25	38	49	56	14	63	20	10	21	19	27	26	45	56	13	48	30
Sr	78	103	34	82	40	102	106	100	138	80	57	81	33	56	339	110	86	57	77	94	152	136
Rb	97	98	196	126	40	97	174	194	153	136	140	125	42	78	28	149	96	47	96	124	227	187
U	5	9	4	15	310	8	41	70	56	5	75	14	5	6	4	4	5	5	4	4	15	20
Th	11	14	6	6	47	13	27	47	24	11	14	5	5	4	4	15	11	10	10	12	14	13
Pb	6	83	4	10	636	82	163	340	383	40	101	9	8	34	6	4	4	4	5	8	9	14
Co	32	19	152	28	66	18	66	74	29	27	60	27	21	14	11	40	22	28	31	27	25	35
Cr	935	885	1750	806	4485	884	1831	2206	1553	1194	1886	805	686	850	310	739	591	810	934	866	677	620
V	233	186	151	166	107	185	200	226	188	201	152	165	52	103	76	191	162	146	232	170	193	178
Ba	405	456	1167	483	192	455	930	1017	933	594	477	482	169	338	158	717	409	228	404	527	1108	935
Sc	34	24	24	21	14	23	25	24	20	27	17	20	8	14	11	31	18	34	33	29	28	28
S	381	5211	450	151	13500	5210	5520	9950	7720	1070	3280	150	630	1030	1260	1940	880	670	380	920	3010	5400
As	8	28	113	13	93	27	226	220	25	34	36	12	8	12	56	250	103	7	7	28	96	96